

8-1-2024

Image Processing Techniques for Water Droplet Penetration Time and Contact Angle Estimation

Sai Balaji Jai Kumar

Follow this and additional works at: <https://digitalscholarship.unlv.edu/thesesdissertations>



Part of the [Artificial Intelligence and Robotics Commons](#), [Computer Engineering Commons](#), [Electrical and Computer Engineering Commons](#), and the [Hydrology Commons](#)

Repository Citation

Jai Kumar, Sai Balaji, "Image Processing Techniques for Water Droplet Penetration Time and Contact Angle Estimation" (2024). *UNLV Theses, Dissertations, Professional Papers, and Capstones*. 5123. <https://digitalscholarship.unlv.edu/thesesdissertations/5123>

This Thesis is protected by copyright and/or related rights. It has been brought to you by Digital Scholarship@UNLV with permission from the rights-holder(s). You are free to use this Thesis in any way that is permitted by the copyright and related rights legislation that applies to your use. For other uses you need to obtain permission from the rights-holder(s) directly, unless additional rights are indicated by a Creative Commons license in the record and/or on the work itself.

This Thesis has been accepted for inclusion in UNLV Theses, Dissertations, Professional Papers, and Capstones by an authorized administrator of Digital Scholarship@UNLV. For more information, please contact digitalscholarship@unlv.edu.

IMAGE PROCESSING TECHNIQUES FOR WATER DROPLET PENETRATION TIME
AND CONTACT ANGLE ESTIMATION

By

Sai Balaji Jai Kumar

Bachelor of Engineering - Electronics and Communication Engineering
Anna University
2019

A thesis submitted in partial fulfilment
of the requirements for the

Master of Science in Engineering – Electrical Engineering

Department of Electrical and Computer Engineering
Howard R. Hughes College of Engineering
The Graduate College

University of Nevada, Las Vegas
August 2024



Thesis Approval

The Graduate College
The University of Nevada, Las Vegas

August 2, 2024

This thesis prepared by

Sai Balaji Jai Kumar

entitled

Image Processing Techniques for Water Droplet Penetration Time and Contact Angle Estimation

is approved in partial fulfillment of the requirements for the degree of

Master of Science in Engineering – Electrical Engineering
Department of Electrical and Computer Engineering

Venkatesan Muthukumar, Ph.D.
Examination Committee Chair

Biswajit Das, Ph.D.
Examination Committee Member

Emma Regentova, Ph.D.
Examination Committee Member

Markus Berli, Ph.D.
Examination Committee Member

Shaikh Arifuzzaman, Ph.D.
Graduate College Faculty Representative

Alyssa Crittenden, Ph.D.
*Vice Provost for Graduate Education &
Dean of the Graduate College*

Abstract

Water droplet behavior on soil surfaces plays a critical role in numerous environmental processes, including soil erosion, hydrological dynamics, and ecosystem health. Accurate characterization of soil water repellency, quantified by parameters such as water droplet penetration time (WDPT) and contact angles (WDCA), is essential for informed decision-making in agricultural management, forestry practices, and land-use planning. Despite the significance of these parameters, challenges exist in reliably estimating them due to the complex and dynamic nature of soil-water interactions.

This thesis address challenges in estimating WDPT and WDCA, by leveraging state-of-the-art image processing techniques and machine learning algorithms. The research focuses on advancing our understanding of water droplet interactions with soil surfaces and developing accurate methods for estimating WDPT and contact angles. Specifically, the thesis explores the utilization of deep machine learning models, such as the YOLOv8 instance segmentation model, for water droplet detection, followed by the application of various deep learning methods for WDPT and contact angle estimation.

The methodology involves the collection of an extensive dataset comprising over 200 samples of water droplets interacting with different soil textures and types. Through rigorous experimentation and model training, the research achieves a remarkable accuracy of 90% in distinguishing between drowning and fully submerged droplets. Comparative analysis with existing techniques further validates the effectiveness of the proposed methodologies. For Water Droplet Penetration Time (WDPT) and Water Droplet Contact Angle (WDCA), the

study demonstrates an error rate below 15% when compared to ground truth data, ensuring the reliability and precision of the approach in analyzing soil-water interactions.

The findings of this study have significant implications for environmental science, hydrological modeling, and agricultural sustainability. By providing reliable tools for characterizing soil water repellency, the research contributes to enhancing environmental management practices and informed decision-making in various fields.

Acknowledgement

I am deeply indebted to my advisor, Dr. Venkatesan Muthukumar, whose unwavering guidance, insightful advice, and continuous encouragement have been instrumental in shaping this research. His expertise and dedication have been a constant source of inspiration and support throughout this journey.

I would like to extend my sincere gratitude to my committee members, Dr. Biswajit Das, Dr. Emma Regentova, Dr. Markus Berli, and Dr. Shaikh Arifuzzaman. Their valuable feedback, and expert insights have greatly enriched this work, helping me refine and improve my research.

Special recognition goes to Adhee Zeidman for her diligent efforts in preparing the soil samples, which were critical for the experimental phase of this study. Her meticulous work and attention to detail have been crucial to the success of the experiments.

I am also profoundly thankful to my lab mates, Mugundan Prakash, Prathibha Shoba, and others, for their constant support, insightful discussions, and collaborative spirit. Their contributions and camaraderie have greatly enhanced the research environment.

Finally, I would like to express my deepest gratitude to my family and friends for their unwavering support and encouragement. Their belief in me has been a driving force throughout this journey, providing me with the strength and perseverance needed to complete this research.

Table of Contents

| | |
|--|-------------|
| Abstract | iii |
| Acknowledgement | v |
| Table of Contents | vi |
| List of Tables | viii |
| List of Figures | ix |
| Chapter 01: Introduction | 1 |
| 1.1 The Necessity of Water Droplet Penetration Time (WDPT) | 1 |
| 1.2 Importance of WDPT in Environmental Management | 1 |
| 1.3 Historical Measurement Methods of WDPT | 2 |
| 1.4 Advances in Technology for Measuring WDPT | 4 |
| 1.5 Ecological and Hydrological Implications of WDPT | 5 |
| 1.6 Global Environmental Health and WDPT | 5 |
| 1.7 Research and Development | 5 |
| Chapter 02: Literature Review | 7 |
| 2.1 Previous Work | 7 |
| 2.2 Our Approach | 8 |
| Chapter 03: Methodology | 10 |
| 3.1 Hardware Setup | 10 |
| 3.2 Data Collection | 11 |
| 3.3 Image Processing using YOLOv8 | 14 |
| 3.4 Soil Preparation | 20 |
| 3.5 X-Delta Arm Robot | 22 |
| Chapter 04: Model Detection | 25 |
| 4.1 Droplet Class Detection | 25 |
| 4.2 Bounding Box Coordinates | 28 |
| 4.3 WDPT Calculation | 29 |
| 4.4 Contact Angle Measurement | 31 |
| 4.5 Mask & Contour Points | 34 |

| | |
|---|-----------|
| Chapter 05: Results & Evaluation | 37 |
| 5.1 YOLOv8 vs. Mask R-CNN Results | 37 |
| 5.2 Bounding Box Coordinates Results | 42 |
| 5.3 Contact Angle Results | 44 |
| 5.4 Water Drop Penetration Time Analysis | 50 |
| 5.5 Volume Analysis | 55 |
| Chapter 06: Conclusion | 59 |
| Appendix | 61 |
| References | 62 |
| Curriculum Vitae | 69 |

List of Tables

| | |
|---|----|
| Table 1: Number of Samples Recorded for Each Soil Type | 13 |
| Table 2: Average Water Absorption Times for Different Hydrophobicity Levels | 13 |
| Table 3: Comparison of Confidence Score (Drowning vs Fully Drowned) | 27 |
| Table 4: Model Comparison Metrics | 38 |
| Table 5: YOLOv8 vs Mask R-CNN: Precision-Recall Comparison | 39 |
| Table 6: Bounding Box Data for 25% Reheated Sand & 40% Lysimeter Soil | 42 |
| Table 7: Angle Comparison of Water Droplet | 44 |
| Table 8: Water Droplet Angles for 25% Reheated Sand & 40% Lysimeter Soil | 48 |
| Table 9: Model Prediction vs Ground Truth for Different Soil/Sand Samples | 51 |
| Table 10: Model Prediction vs Ground Truth for 25% Reheated Sand | 52 |
| Table 11: Distribution of White/Lysimeter Soil Samples | 53 |
| Table 12: Comparison of Volume Calculations 100% Lysimeter Soil | 57 |

List of Figures

| | |
|---|----|
| Figure 1: WDPT Manual Test | 2 |
| Figure 2: WDPT System Core Setup | 11 |
| Figure 3: Recorded Image Sequences | 12 |
| Figure 4: Annotation of Water Droplet | 15 |
| Figure 5: F1 Confidence Curve | 16 |
| Figure 6: Precision-Confidence Curve | 17 |
| Figure 7: Visual Segmentation Output | 18 |
| Figure 8: Different Types of Soil Samples Used | 21 |
| Figure 9: Setup of X-Delta Arm Robot | 23 |
| Figure 10: Model Drowning Detection | 25 |
| Figure 11: Model Fully Drowned Detection | 26 |
| Figure 12: Terminal Output Displaying Bounding Box Coordinates | 28 |
| Figure 13: Penetration Time Terminal Output | 31 |
| Figure 14: Real-Time Contact Angle Measurement of the Droplet | 34 |
| Figure 15: Contour Points of the Droplet | 35 |
| Figure 16: Mask of the Droplet | 36 |
| Figure 17: Precision-Recall Graph for YOLOv8 and Mask R-CNN | 40 |
| Figure 18: Flowchart of YOLOv8 and Mask R-CNN processes | 41 |
| Figure 19: Bounding Box Graph for 25% Reheated Sand & 40% Lysimeter soil | 43 |
| Figure 20: Graphical Representation of the Contact Angles Points | 45 |
| Figure 21: Contact Angle Graph for 25% Reheated Sand and 40% Lysimeter soil | 49 |
| Figure 22: Sample Distribution of White/Lysimeter Soil Samples | 54 |

Chapter 01: Introduction

1.1 The Necessity of Water Droplet Penetration Time (WDPT)

Water Droplet Penetration Time (WDPT) and Water Droplet Contact Angle (WDCA) is a crucial metric in soil science, pivotal for assessing soil water repellency (SWR) [1], which has profound implications for environmental management, agriculture, and ecological conservation [2]. This expanded discussion explores the necessity of WDPT, its historical measurement methods, the evolution of technology in its assessment, and its broader environmental implications.

1.2 Importance of WDPT in Environmental Management

WDPT is essential for accurately assessing the hydrophobicity of soils, particularly in environments affected by wildfires [3] or in agricultural [4] where irrigation practices are critical. Soil water repellency leads to reduced water infiltration, which can increase surface runoff, enhance soil erosion risks, and decrease water availability for plants. This phenomenon is critical in managing post-wildfire landscapes [5] where the soil can become significantly hydrophobic, preventing effective water absorption and increasing the risk of flash floods and mudslides [6]. For instance, following significant wildfires, such as the one on Mount Pellegrino in 2016, rapid assessment of SWR was crucial to predict potential hydrological consequences and implement necessary mitigation actions to safeguard affected communities.

1.3 Historical Measurement Methods of WDPT

The traditional methodologies for measuring Water Droplet Penetration Time (WDPT) have evolved significantly over the years, yet they all share a common goal: to assess the degree of water repellency in soils. Initially, WDPT was measured manually as shown in Figure 1, a method that, while straightforward, presented numerous challenges related to accuracy and consistency.



Figure 1: WDPT Manual Test

Early methods involved simply observing and timing how long it took for a water droplet to infiltrate the soil surface [7]. This manual technique was one of the simplest forms of measuring soil water repellency but was highly susceptible to observational biases and environmental influences such as wind and temperature, which could alter the droplet's behavior and the measurement's accuracy.

As the need for more precise and reliable measurements became apparent, researchers developed more standardized approaches. The Water Drop Penetration Time (WDPT) test, as formalized by researchers like Doerr et al [8], became a foundational method. This test involves placing a standard volume of water on the soil surface and using a stopwatch to measure the time taken for complete absorption. This method provided a more quantifiable approach to assessing soil hydrophobicity but still relied heavily on manual timing and could be influenced by the droplet's size and the soil's surface condition.

To address these limitations, subsequent innovations included the use of more controlled droplet application techniques and environmental controls during testing. Studies compared various application methods, such as using manual versus automated droplet dispensers, to improve the consistency and reliability of measurements. Automated systems allowed for more precise control over droplet size and the timing of its application, reducing the variability caused by manual operation and providing a more consistent basis for comparison across different soil types and conditions [9].

Additionally, the integration of digital timers and high-resolution video recording equipment further enhanced the precision of WDPT measurements. These tools allowed researchers to capture and analyze the infiltration process in real-time, providing detailed data that could be used to better understand the dynamic interaction between water droplets and soil particles. The use of video analysis also facilitated the study of the initial contact angle and the rate of change over time, adding another layer of depth to the understanding of soil hydrophobicity [10].

1.4 Advances in Technology for Measuring WDPT

Our research contributes significantly to the measurement of Water Droplet Penetration Time (WDPT), with increased precision and reliability. Central to our approach is the integration of automated systems for controlled water droplet delivery and cutting-edge imaging technologies to estimate WDPT. The key components of our system include an electronic pipette, single board computer, and high-definition cameras. These technologies coalesce to automate and refine the process of WDPT measurements, ensuring controlled droplet release and exact timing.

Automation plays a pivotal role in our methodology, mitigating human error and bolstering the consistency of our measurements. The high-definition cameras we employ are crucial for capturing the complex interactions between water droplets and soil. This data is not merely descriptive but analytical, offering deep insights into the soil's behavior under varying environmental conditions. The level of detail in our imagery elucidates both the immediate absorption rates and the intricate dynamics of how water interacts with diverse soil textures.

Moreover, the adaptability of our systems to unmanned aerial vehicles (UAVs), or drones, revolutionizes our field studies. These drones can traverse and assess remote or difficult terrains, enabling extensive soil health evaluations without direct human intervention. This capability is invaluable for conducting ecological studies in areas susceptible to natural disturbances or managing large agricultural lands efficiently. By harnessing these technological advancements, our team is equipped to perform thorough and expansive assessments of soil water repellency, significantly enhancing decision-making processes for environmental management and agricultural optimization.

1.5 Ecological and Hydrological Implications of WDPT

In ecological and hydrological studies, WDPT measurements are vital for maintaining the natural balance of ecosystems, particularly in sensitive environments like wetlands where water infiltration rates significantly affect the habitat's water table and, consequently, its plant and animal life [11]. Precise WDPT measurements enable the design of effective conservation strategies, ensuring that necessary water levels are maintained to support these delicate ecosystems [12].

1.6 Global Environmental Health and WDPT

On a broader scale, accurate WDPT measurements are crucial for addressing global challenges such as climate change and sustainable land management [13]. Areas undergoing desertification, for instance, can benefit from targeted WDPT studies that lead to better soil management practices [14], potentially reversing land degradation trends and promoting healthier, more resilient soil ecosystems. These practices are integral to global efforts aimed at enhancing food security, managing water resources, and preserving the ecological balance [15].

1.7 Research and Development

The academic and practical applications of Water Droplet Penetration Time (WDPT) are extensive, particularly in understanding and mitigating the effects of wildfires on soil properties. Recent studies have highlighted the critical impact of post-fire conditions on soil hydrophobicity and the necessity of precise WDPT measurements. For instance, the 2021 Caldor Megafire in the Eastern Sierra Nevada significantly altered soil properties, with WDPT and apparent contact angle measurements documenting increased soil hydrophobicity [16]. These findings underscore the importance of WDPT in post-fire soil assessments, facilitating

the development of effective soil rehabilitation strategies. Similarly, research on the Gangneung Forest fire in South Korea demonstrated how severe burns exacerbate soil water repellency, emphasizing the role of accurate WDPT measurements in ecological recovery efforts [17].

Technological advancements have further enhanced WDPT measurement techniques. Automated systems equipped with high-definition cameras and precision droplet applicators, such as the Mini-Disk Infiltrometer (MDI), offer greater accuracy and consistency compared to traditional methods. These systems are particularly useful in post-fire landscapes, where rapid and precise assessments guide soil restoration efforts [18]. Additionally, integrating machine learning algorithms with WDPT measurement systems has improved efficiency and reliability [19]. Deep learning models, like Convolutional Neural Networks (CNNs), enable real-time analysis of droplet interactions with soil, providing detailed insights into the effects of fire on soil properties [20].

Chapter 02: Literature Review

2.1 Previous Work

The characterization of soil water repellency has been the focus of extensive research, with various methodologies developed to assess this critical property. Traditional methods include the Water Drop Penetration Time (WDPT) test, contact angle measurements, and the molarity of ethanol droplet (MED) test [21]. These methods have been widely employed due to their ability to provide direct measurements of soil hydrophobicity. WDPT, for example, has been a popular method for its straightforward application, despite limitations related to human error and environmental variability.

Research has also delved into the effectiveness of different application techniques for WDPT. For instance, in fire-affected regions of Sicily [22], various methods such as manual spraying, automated spraying, and immersion have been compared. These studies found that automated methods generally offer better consistency and efficiency, though manual methods can still be effective depending on the specific conditions. The importance of choosing the appropriate application method is emphasized, particularly in contexts with varying soil moisture content, temperature, and surface roughness.

In the lower Himalayan regions of India [23], studies have explored the impact of land use on soil water repellency. Using WDPT and other characterization methods, researchers assessed soil samples from forests, agricultural fields, and urban areas. They found significant variations in water repellency based on land use, highlighting how human activities and land management practices can alter soil properties and affect water management strategies.

The integration of advanced technologies has also been a significant focus. Deep Convolutional Neural Networks (CNNs) have been employed to segment images of droplet deposition, improving the accuracy and efficiency of spray distribution assessments [24]. This method showcases the potential of machine learning to enhance traditional soil assessment techniques, providing more precise and detailed data. Furthermore, a survey of water droplet recognition algorithms has evaluated various approaches, including thresholding, edge detection, and machine learning-based methods. This comprehensive analysis helps in selecting the most suitable techniques for different scenarios, contributing to the development of more reliable water droplet recognition systems.

In Sicily, studies conducted two years post-fire [25] have used WDPT to assess soil water repellency, aiming to understand the persistence of hydrophobicity and its impact on soil hydrology. These studies highlight the importance of long-term monitoring of soil properties following environmental disturbances to inform soil management and restoration efforts. Similarly, research on hydrophobized sand has examined water repellency indices, including WDPT, providing insights into the hydrophobicity of treated surfaces and their potential applications in various environmental and agricultural areas.

2.2 Our Approach

Our approach in measuring Water Droplet Penetration Time (WDPT) introduces several innovative advancements over traditional methods. Unlike the conventional techniques that rely heavily on manual timing and subjective assessments, our system integrates automation and deep machine learning technologies to enhance measurement accuracy and efficiency.

We utilize the Pluto valve, an off-the-shelf electronic pipette, for precise control over droplet release, coupled with the computational power of the Raspberry Pi for real-time data capture. High-definition cameras capture detailed images of water droplets interacting with soil surfaces, which are then analyzed offline using Convolutional Neural Networks (CNNs). Specifically, we employ the YOLOv8 model, a state-of-the-art deep learning algorithm that enables real-time detection and segmentation of water droplets. This automated setup significantly reduces human error and environmental variability, ensuring more reliable and repeatable measurements.

Additionally, our approach is intended to be used on drones equipped with these advanced systems, enabling large-scale assessments of soil water repellency in remote and inaccessible areas. This capability represents a significant improvement over previous methodologies limited to smaller, manually accessible sites. By leveraging these technological advancements, our methodology not only enhances the precision of WDPT measurements but will also improve the scalability and applicability of soil water repellency assessments, providing a robust tool for environmental management and agricultural practices.

Chapter 03: Methodology

3.1 Hardware Setup

The hardware setup for measuring Water Droplet Penetration Time (WDPT) incorporates several advanced components to ensure precise and efficient measurements. At the core of the setup is the electronic pipette [26], which stores water and controls its release. The valve switch is connected to a Raspberry Pi (RPI) through an optocoupler, which protects the RPI reverse current. The Raspberry Pi triggers pulses to open the electronic pipette, allowing for the accurate control of droplet size by adjusting the opening time.

Below the valve is a Petri dish containing soil samples. Multiple soil samples are used to obtain a variety of results, ensuring the robustness of the data. An ArUco marker [27] is placed on top of the soil to aid in pose estimation, ensuring accurate positioning and measurement of the droplets. The ArUco marker is a type of fiducial marker widely used in computer vision applications to determine the orientation and position of objects within the frame. In this setup, the ArUco marker provides a reference point for aligning the camera and the droplet, which is crucial for obtaining consistent and reliable measurements.

The IMX477 camera [28], mounted on a tripod, plays a crucial role in capturing high-definition images of the water droplets as they interact with the soil. The camera's autofocus feature ensures that the images are clear and focused, and it is controlled by the Raspberry Pi to synchronize data capture.

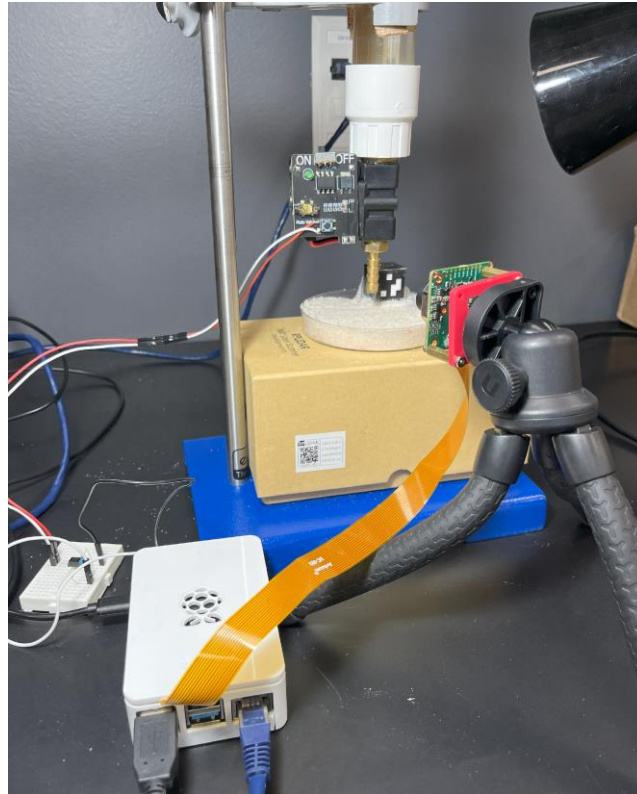


Figure 2: WDPT System Core Setup

To eliminate any background disturbances and enhance the visibility of the water droplets, an external light source is used. This setup ensures that the release and measurement of water droplets are both precise and repeatable, facilitating accurate WDPT assessments in various environmental conditions. The core setup of this system is shown in Figure 2.

3.2 Data Collection

The data collection process involves capturing images and videos of water droplets interacting with various soil types, under different conditions, to study soil properties and train the deep learning model effectively. This comprehensive data collection is crucial for understanding water-soil interactions both in a controlled laboratory setup and in field applications.

The process begins with the electronic pipette, controlled by the Raspberry Pi 4B, which precisely triggers the release of water droplets. The IMX477 high-resolution camera starts capturing video and images just before the droplet leaves the valve and continues until the droplet is completely absorbed by the soil. This entire sequence ensures that the dynamic interaction between the water droplet and the soil surface is thoroughly captured. Videos are recorded in high resolution (720p or 1080p) at 60 or 90 frames per second (fps), for detailed visual data for analysis. An external light source, providing a lux value of 650-750, ensures that the droplets are clearly visible, eliminating background disturbances. During field test we propose to use artificial light under the drone to maintain this lux value. Figure 3 illustrates various images recorded at different sequences during the data collection process.

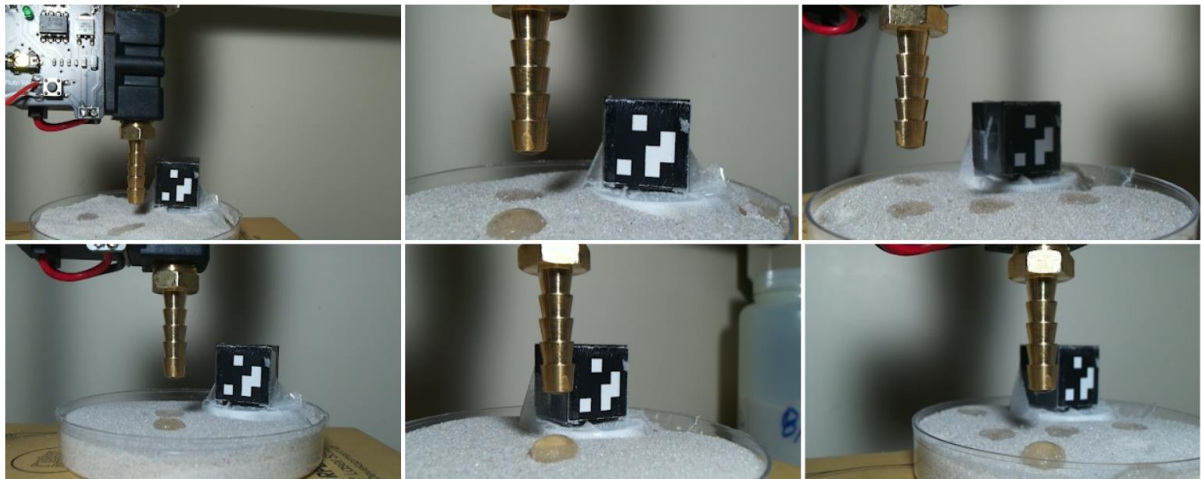


Figure 3: Recorded Image Sequences

In this study, a total of 167 video samples were recorded across different soil types and hydrophobicity levels. These samples include various soil conditions such as Lysimeter Soil [29], Pink Sand [30], Reheated Sand [31], and White Sand [32] with varying hydrophobicity percentages. The average duration of these video samples ranged from 30 seconds to 150

seconds, and most were recorded at a resolution of 720p or 1080p. Pink Sand was recorded the least because the soil-water interaction did not alter much, making it less relevant for extensive analysis. Table 1 summarizes the number of videos recorded for each soil type.

Table 1: Number of Samples Recorded for Each Soil Type

| Soil Type | No of Samples Recorded |
|------------------|-------------------------------|
| Lysimeter Soil | 86 |
| Pink Sand | 6 |
| Reheated Sand | 53 |
| White Sand (30%) | 22 |
| Total | 167 |

The hydrophobicity of the soil significantly influences the absorption time of water droplets.

Table 2 [23] below illustrates the average water absorption times.

Table 2: Average Water Absorption Times for Different Hydrophobicity Levels

| Water repellency | WDPT (s) |
|----------------------------------|-----------------|
| Wettable | <5 |
| Slightly to moderately repellent | 5–60 |
| Strongly water-repellent | 60–600 |
| Severely water-repellent | 600–3600 |

The results demonstrate that lower hydrophobicity leads to quicker water absorption, while higher hydrophobicity increases the absorption time.

3.3 Image Processing using YOLOv8

YOLOv8 (You Only Look Once, Version 8) is the latest iteration of the YOLO object detection model developed by Ultralytics [33]. Renowned for its superior accuracy and efficiency in real-time applications, YOLOv8 integrates advanced deep learning and computer vision technologies to enhance its performance in tasks such as detection, segmentation, and classification. Building on the strengths of its predecessors, YOLOv8 offers a streamlined design and remarkable flexibility, making it suitable for deployment on various hardware platforms, from edge devices to cloud APIs. This versatility is particularly beneficial for our application involving water droplet detection in soil analysis, where real-time detection and segmentation of water droplets are crucial for accurate hydrophobicity assessments.

The model supports a wide range of vision AI tasks, ensuring precise and real-time detection and segmentation of water droplets. By leveraging YOLOv8, we achieve high accuracy and scalability, significantly advancing our research in soil water repellency measurements. This capability allows us to conduct thorough analyses and obtain reliable data essential for understanding soil-water interactions.

Data Preparation and Model Training

After data collection, the captured images and videos are systematically sorted into three categories: test, train, and validation datasets. This sorting process is critical for training the YOLOv8 model effectively. The primary purpose of using YOLOv8 for droplet detection is to

measure various parameters such as droplet penetration time, contact angle, and droplet coordinates in the recorded frames.

For this study, we trained YOLOv8 using over 200 images representing different soil types and droplet conditions. The first step involves using an annotation software called "LabelMe" [34] to highlight the droplets against the background. As shown in Figure 4, the software allows us to create polygons around the droplets, which helps in distinguishing between two classes: "Drowning" and "Fully Drowned," depending on their absorption stages. These annotations are crucial for training the model to recognize and segment droplets accurately.

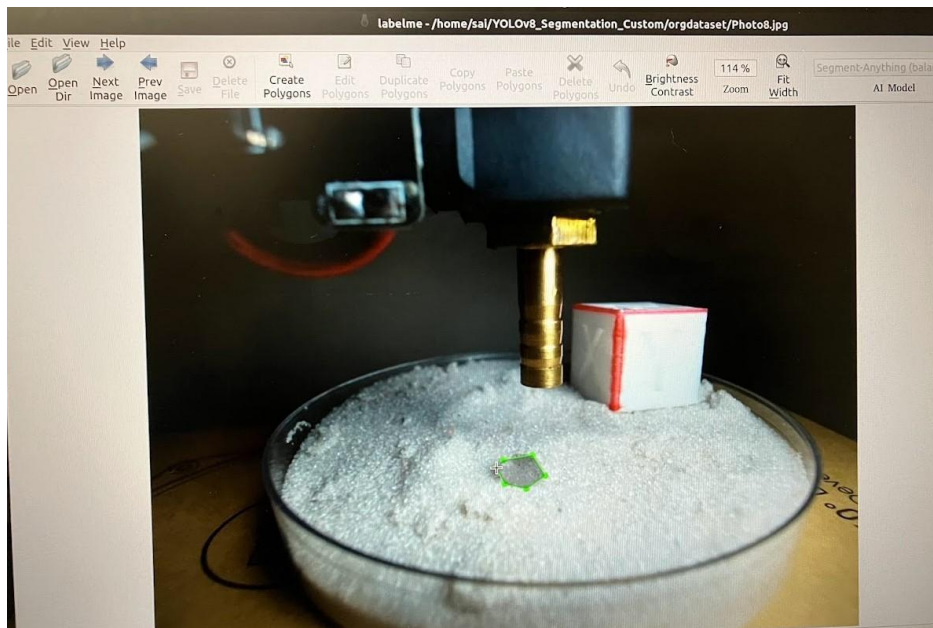


Figure 4: Annotation of Water Droplet

Once the annotations are completed, the files are converted into a format that YOLOv8 can understand. The annotated files, along with the dataset images, are then divided into three folders: test, train, and validation. This division ensures that the model is trained on a diverse

set of images, enhancing its ability to generalize and perform well on unseen data. The model is trained for 100 epochs with images set to a resolution of 640 pixels, optimizing the model's parameters for best performance.

Training Results and Model Evaluation

Upon completing the training process, the model's performance is evaluated using various metrics. One of the key evaluation tools is the F1 Confidence Curve, shown in Figure 5. This graph illustrates the relationship between confidence score thresholds and F1-scores, helping in selecting an optimal threshold that balances precision and recall [35].

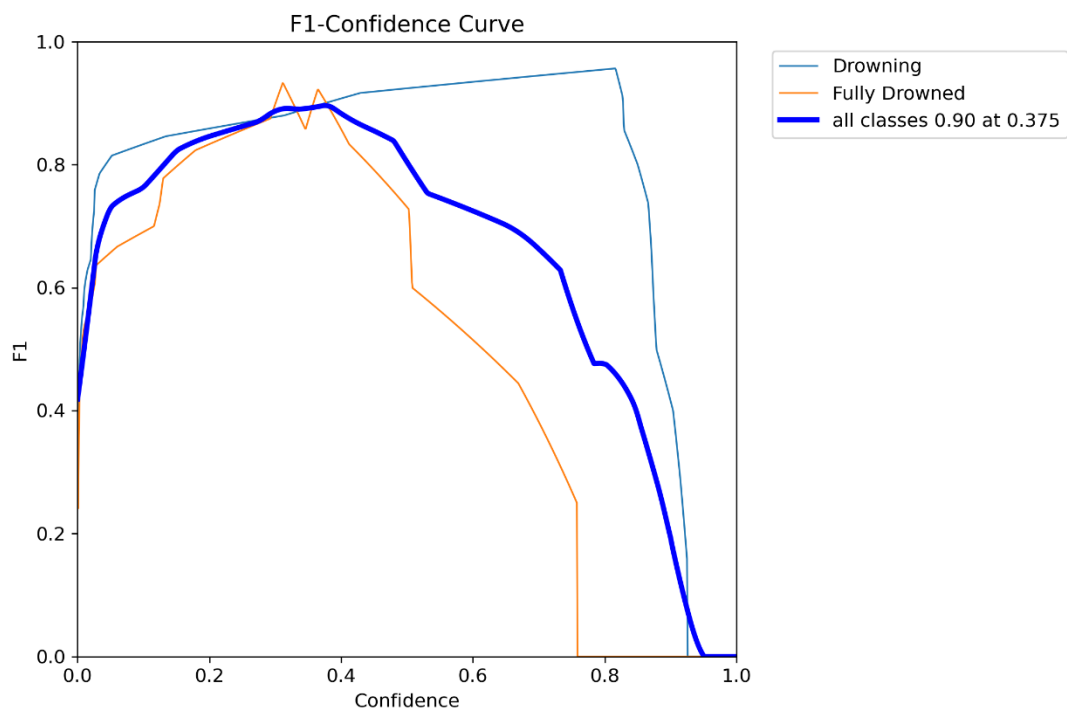


Figure 5: F1 Confidence Curve

Mathematically, the F1 score is a weighted harmonic mean of precision and recall, ranging from 0 to 1, with 1 being the best possible score:

$$F1 = 2 * (precision * recall) / (precision + recall)$$

The Precision Confidence Curve graph (Figure 6) further aids in understanding how precision varies with confidence score thresholds, providing insights into the accuracy of the model's predictions.

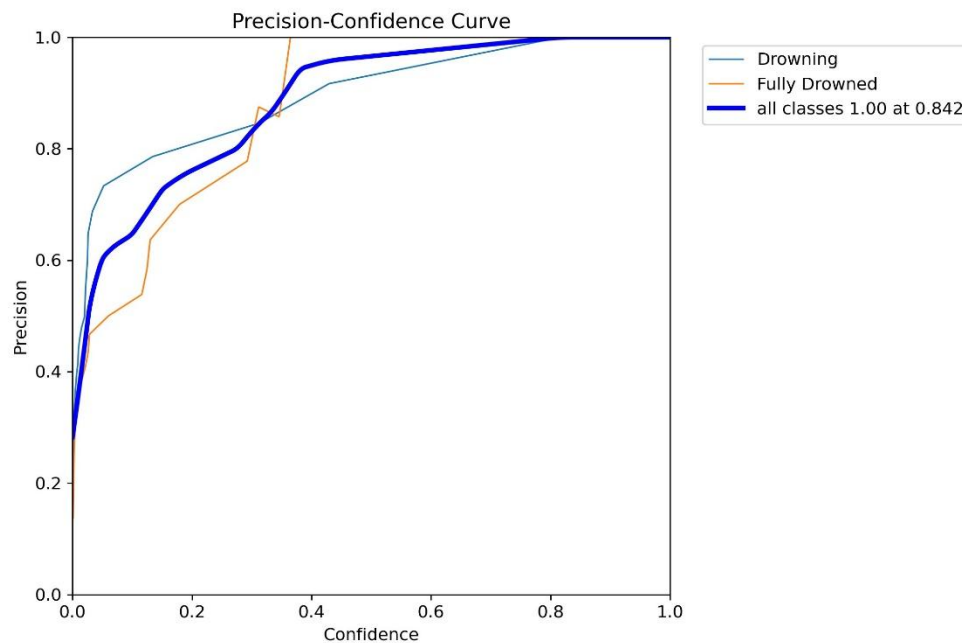


Figure 6: Precision-Confidence Curve

Visualizing segmentation masks is another essential aspect of model evaluation. These masks offer a detailed view of how the model perceives water droplets and their absorption stages. The segmentation output distinguishes between "Drowning" and "Fully Drowned" droplets, as

shown in Figure 7. This visualization not only validates the model's performance but also helps in refining the detection and segmentation processes.

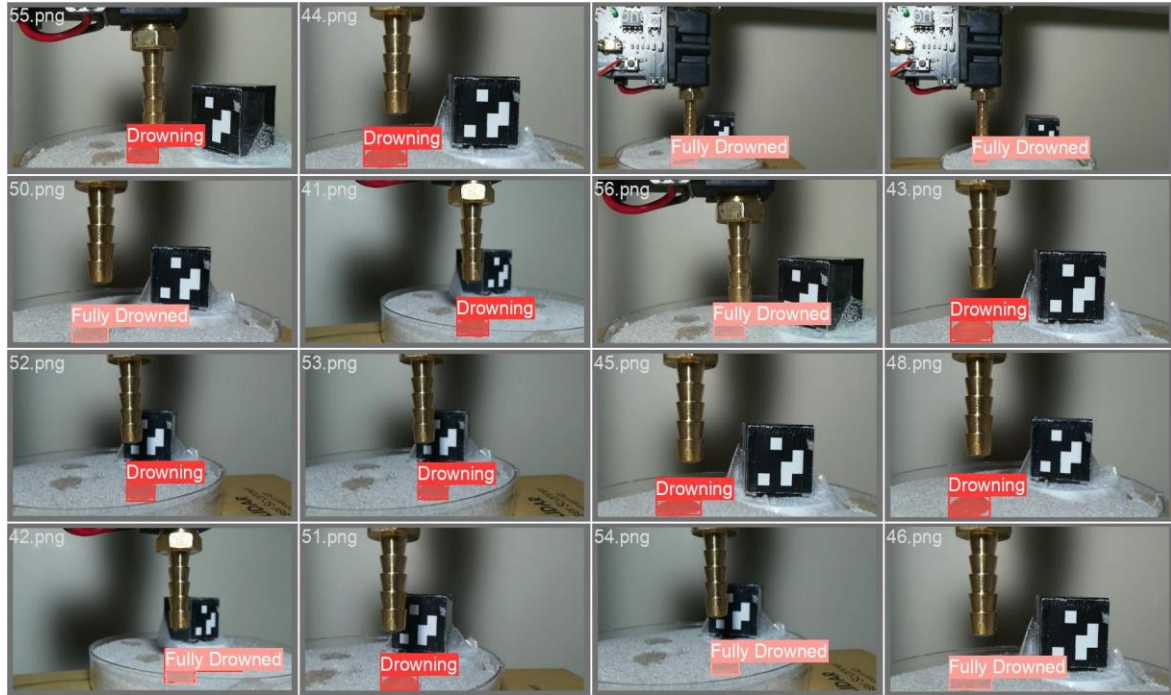


Figure 7: Visual Segmentation Output

The integration of YOLOv8 into our research framework significantly enhances the precision and efficiency of water droplet detection and segmentation. The detailed data preparation and rigorous training processes ensure that the model performs reliably across various conditions, thereby advancing our understanding of soil hydrophobicity and its implications for environmental and agricultural management.

Mask R-CNN:

Mask R-CNN (Region-based Convolutional Neural Networks) is a powerful and versatile model for object detection, segmentation, and classification. Developed as an extension of Faster R-CNN, Mask R-CNN enhances the capabilities of its predecessor by introducing an additional branch that predicts segmentation masks for each Region of Interest (RoI). This branch operates in parallel with the existing branches that handle classification and bounding box regression, making Mask R-CNN adept at performing multiple tasks simultaneously.

The architecture of Mask R-CNN consists of several key components:

- **Backbone Network:** The backbone network, typically a ResNet or ResNeXt, is used for feature extraction. It generates feature maps from the input image, capturing important spatial information.
- **Region Proposal Network (RPN):** The RPN generates candidate object proposals by sliding a small network over the feature maps. It predicts object scores and refines bounding boxes, which are then used to identify potential objects in the image.
- **RoI Align:** RoI Align is a critical component that improves upon the RoI Pooling used in Faster R-CNN. It ensures that the regions of interest are properly aligned with the

feature maps, preserving spatial accuracy and improving the precision of object detection and segmentation.

- **Classification and Bounding Box Regression:** For each RoI, the model predicts the class label and refines the bounding box coordinates, allowing for accurate object localization and classification.
- **Segmentation Masks:** The additional branch in Mask R-CNN predicts a binary mask for each RoI. This mask indicates the pixel-level segmentation of the object, enabling precise delineation of object boundaries.

By integrating segmentation capabilities with object detection, Mask R-CNN offers a comprehensive solution for analyzing the interaction between water droplets and soil. This capability is crucial for understanding soil hydrophobicity and water repellency, as the segmentation masks help visualize how droplets interact with different soil types.

3.4 Soil Preparation

The preparation of soil samples is a critical step in ensuring the accuracy and reliability of Water Droplet Penetration Time (WDPT) measurements. This section details the methods and protocols used to prepare the soil samples for our experiments, which included various types of soil with different hydrophobicity levels.

For all experiments in this study, a medium-fine silica sand with a diameter range of 0.595–0.125 mm was selected as the soil surrogate. This specific sand, sourced from AGSCO Corporation, Wheeling, IL, USA, has been used in similar studies on soil-water repellency (SWR) and soil hydraulic properties [30]. The preparation steps for the silica sand involved a thorough cleaning process using a 0.003 M hydrochloric acid solution (Fisher Scientific, Fair Lawn, NJ, USA) to remove impurities and potential contaminants. Following the acid cleaning, the sand was extensively rinsed with ultra-high purity water ($18 \text{ M}\Omega \text{ cm}^{-1}$) produced by an ELGA water system (ELGA® LabWater, Woodridge, IL, USA).

Post-cleaning, the sand was placed into a tray covered with aluminium foil and dried in an oven at 105°C for 48 hours. This process ensured the removal of any residual moisture and acid, resulting in untreated or “0%” sand, which served as the baseline for further soil preparations. The key physical and chemical properties of the prepared soil samples include a particle size range of 0.595–0.125 mm diameter, neutralized acidity post-cleaning, and negligible moisture content after drying at 105°C .



Figure 8: Different Types of Soil Samples Used

To create samples with varying hydrophobicity levels, additional treatments were applied to the baseline sand. For instance, to prepare pink sand, the untreated 0% sand was dyed with Rhodamine B dye and subjected to the same drying process at 105 °C for 48 hours. After drying, the dyed sand was placed in a desiccator for an additional 24 hours to stabilize the dye. Furthermore, to create mixed sand samples, the 0% sand was mixed with pink sand by percentage mass, ensuring controlled variations in hydrophobicity. Figure 8 shows the various types of sample soil used during the WDPT process.

The preparation of Lysimeter soil involved collecting samples from the field at a depth of 0-20 cm and sifting them using a common colander to remove larger stones and ensure uniformity. This sifting process was essential for maintaining consistent experimental conditions across all soil samples.

Standard procedures and protocols were meticulously followed throughout the soil preparation process to maintain consistency and reproducibility. These protocols included the use of 0.003 M hydrochloric acid for cleaning, ultra-high purity water for rinsing, and oven drying at 105 °C for 48 hours in aluminium foil-covered trays. Additionally, the dyeing process involved adding Rhodamine B dye to the sand, followed by stabilization in a desiccator to ensure uniform dye distribution.

3.5 X-Delta Arm Robot

The X-Delta Arm Robot [36] is an integral component of our experimental setup, designed to ensure precise control over the water droplet delivery process. This robotic arm is equipped with an electronic pipette, which is crucial for controlling the release of water droplets onto the soil samples.

The X-Delta Arm Robot can move the electronic pipette in the x, y, and z axes, providing versatile positioning capabilities. This movement is facilitated by three Dynamixel stepper motors [37], which offer high precision and reliability. The ability to adjust the valve's position in three dimensions allows for accurate targeting of the soil sample, ensuring that the droplet is delivered to the desired location without any deviation.

One of the critical functionalities of the X-Delta Arm Robot is its capability to adjust the height of the electronic pipette. This adjustment is vital to ensure that the water droplet falls onto the soil sample without bouncing, which could otherwise affect the accuracy of the WDPT measurements. By maintaining an optimal height, the arm ensures that the droplet impacts the soil with minimal disturbance.



Figure 9: Setup of X-Delta Arm Robot

Figure 9 shows the complete setup, casing of the X-Delta Arm Robot, the electronic pipette, the IMX477 camera, and the control modules. This setup represents a versatile system for conducting precise and controlled WDPT measurements.

The entire setup, DropMLAB, includes the Pluto valve, X-Delta Arm Robot, IMX477 camera, and control modules. This enclosure is designed to eliminate any external lighting effects that could interfere with the droplet detection and measurement process. By creating a controlled environment, the enclosed box ensures that the experiments are conducted under consistent lighting conditions, thereby enhancing the reliability of the results.

For field experiments, this setup will be attached to the bottom of a drone. This mobile configuration allows us to carry out experiments in remote forest areas, providing valuable data on soil water repellency in various environmental conditions. The ability to transport the setup to different locations expands the scope of our research, enabling us to study soil hydrophobicity in diverse terrains and climates.

Chapter 04: Model Detection

4.1 Droplet Class Detection

The YOLOv8 model plays a critical role in detecting and labelling water droplets as they interact with soil. Once a droplet falls onto the soil, the YOLOv8 model picks up the droplet's structure and starts labelling it as "Drowning" (Figure 10). Bounding boxes and droplet contours appear around the droplet, dynamically adjusting as the droplet size changes. The confidence score, displayed alongside the label, provides a measure of the model's certainty in its detection. A threshold of 0.5 is maintained to ensure the reliability of detections.

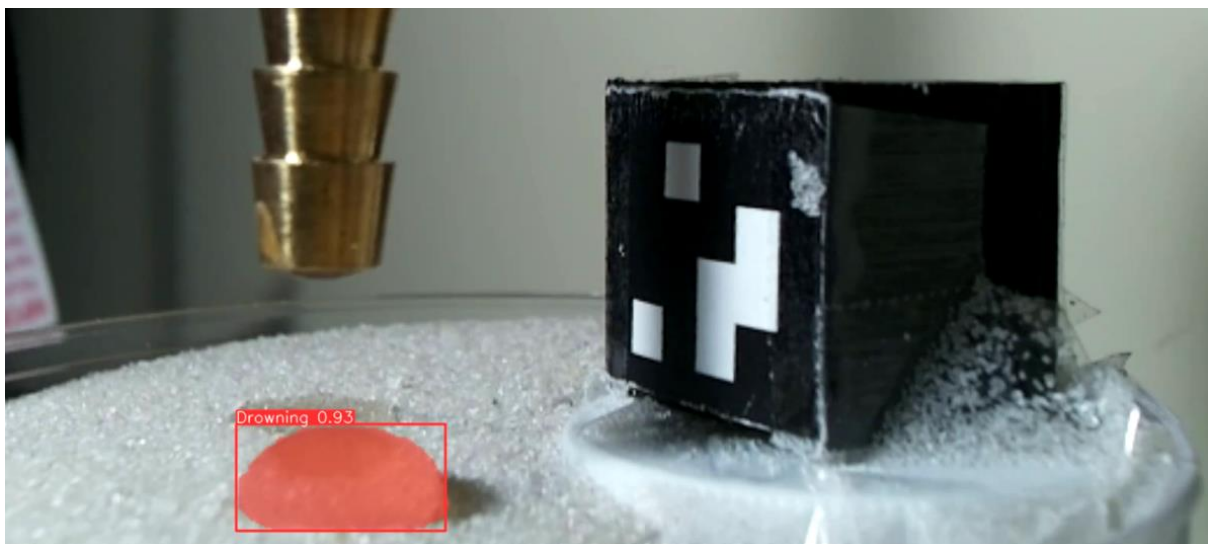


Figure 10: Model Drowning Detection

This detection process is performed in real time, allowing continuous monitoring of the droplet's behavior. As the droplet is absorbed by the soil, the bounding box's size decreases until the droplet is fully absorbed. At this point, the model labels the droplet as "Fully Drowned," as shown in Figure 11 marking the transition and updating the bounding box and

confidence score accordingly. This detection capability is crucial for determining the water droplet penetration time (WDPT) and performing volume analysis.



Figure 11: Model Fully Drowned Detection

Table 3 below compares the average confidence scores between the "Drowning" and "Fully Drowned" classes across five different test samples. The scores demonstrate the model's effectiveness and suitability for this type of research.

Table 3: Comparison of Confidence Score (Drowning vs Fully Drowned)

| Test Sample | Soil Type | Drowning Class Avg (%) | Fully Drowned Avg (%) |
|-------------|------------------------|---------------------------|--------------------------|
| Sample 1 | 0% Lysimeter Soil | - | 82 |
| Sample 2 | 25% Reheated Sand | 87 | 90 |
| Sample 3 | 30% White Sand | 93 | 89 |
| Sample 4 | 40% Lysimeter Soil | 92 | 88 |
| Sample 5 | 50% Lysimeter Soil | 86 | 83 |
| Sample 6 | 100% Lysimeter Soil | 95 | - |

The table illustrates the model's high confidence scores in detecting both the "Drowning" and "Fully Drowned" states of the droplets, underscoring its effectiveness for this application. The confidence scores clearly indicate the reliability and precision of the YOLOv8 model in tracking the droplet absorption process, making it an invaluable tool for analyzing soil hydrophobicity and water penetration properties.

4.2 Bounding Box Coordinates

Bounding box coordinates of the water droplet are crucial for accurately locating the water droplet within each frame of the captured video. These coordinates are not only essential for detection but also play a vital role in the subsequent volumetric analysis of the droplet.

To extract the bounding box coordinates, a Python script is employed that processes the output generated by the YOLOv8 model for each frame. The YOLOv8 model provides these coordinates in the form of tensors, which represent the bounding box around the detected droplet. The format for these coordinates is [x_min, y_min, x_max, y_max], indicating the top-left and bottom-right corners of the bounding box.

The extracted bounding box coordinates are then used to calculate various parameters needed for volume analysis and to monitor the droplet's behavior as it interacts with the soil. This information is vital for understanding the droplet absorption process and the soil's hydrophobic properties.

```
(yolov8_segmentation) bigboy@bigboy-Precision-7560:~/Desktop/Yolov8_Segmentation_Custom$ python predict00.py
WARNING ⚠️ 'line_thickness' is deprecated and will be removed in 'ultralytics 8.2' in the future. Please use 'line_width' instead.

image 1/1 /home/bigboy/Desktop/Yolov8_Segmentation_Custom/1.png: 384x640 1 Drowning, 84.7ms
Speed: 1.3ms preprocess, 84.7ms inference, 231.1ms postprocess per image at shape (1, 3, 384, 640)
Results saved to runs/segment/predict118
1 label saved to runs/segment/predict118/labels
ultralytics.engine.results.Boxes object with attributes:

cls: tensor([0.], device='cuda:0')
conf: tensor([0.8626], device='cuda:0')
data: tensor([[660.1999, 769.0467, 843.6962, 858.8508, 0.8626, 0.0000]], device='cuda:0')
id: None
is_track: False
orig_shape: (895, 1615)
shape: torch.Size([1, 6])
xywh: tensor([[751.9480, 813.9487, 183.4963, 89.8041]], device='cuda:0')
xywhn: tensor([[0.4656, 0.9094, 0.1136, 0.1003]], device='cuda:0')
xyxy: tensor([[660.1999, 769.0467, 843.6962, 858.8508]], device='cuda:0')
xyxyn: tensor([[0.4088, 0.8593, 0.5224, 0.9596]], device='cuda:0')
```

Figure 12: Terminal Output Displaying Bounding Box Coordinates

Figure 12, illustrates the terminal output of the script, showcasing the tensor values which denote the bounding box coordinates. These values are dynamically updated for each frame, providing real-time tracking of the droplet.

By utilizing these coordinates, we can accurately track the droplet's position and size, which is essential for detailed analysis and research on soil hydrophobicity and water droplet penetration time. The precision of the bounding box coordinates ensures that the detection and analysis are reliable and can be used to derive meaningful conclusions.

4.3 WDPT Calculation

The process of calculating WDPT involves several steps, from the detection of the water droplet by the YOLOv8 model to the final computation of the penetration time. The YOLOv8 model plays a vital role in this process by accurately detecting and classifying the state of the water droplet as it interacts with the soil.

The process begins with initializing the YOLOv8 model, specifically trained for segmentation tasks using a custom weight file ("yolov8m-seg-custom.pt"). The model is applied to each frame of the video capturing the droplet's interaction with the soil. This real-time detection ensures that the droplet's shape and position are continuously monitored as it interacts with the soil surface.

Classification: When a water droplet falls onto the soil sample, the YOLOv8 model identifies and labels the droplet with the class "Drowning". This detection is performed in real-time, with the model continuously updating the bounding box coordinates and the confidence score as the droplet changes shape and size. The classification of the droplet as "Drowning" indicates that the droplet is in the process of being absorbed by the soil. As the droplet continues to be absorbed, the YOLOv8 model monitors its status until the point where the droplet is no longer visible or has been completely absorbed by the soil. At this stage, the model changes the label from "Drowning" to "Fully Drowned". This transition is crucial as it marks the end of the water droplet penetration process.

Logging Detection Data: Throughout the detection process, the YOLOv8 model outputs various detection values, including the class labels, bounding box coordinates, and confidence scores. These values are displayed in the terminal and simultaneously saved as a log file. The log file records the detection data for each frame, capturing the moment the droplet is first labelled as "Drowning" and the moment it changes to "Fully Drowned".

Python Script for WDPT Calculation: To calculate the WDPT, a Python script is employed to process the log file generated by the YOLOv8 model. The script reads the log file and identifies the frame time of the first instance of the "Drowning" class and the frame time just before the label changes to "Fully Drowned". These frame times represent the start and end points of the water droplet penetration process.

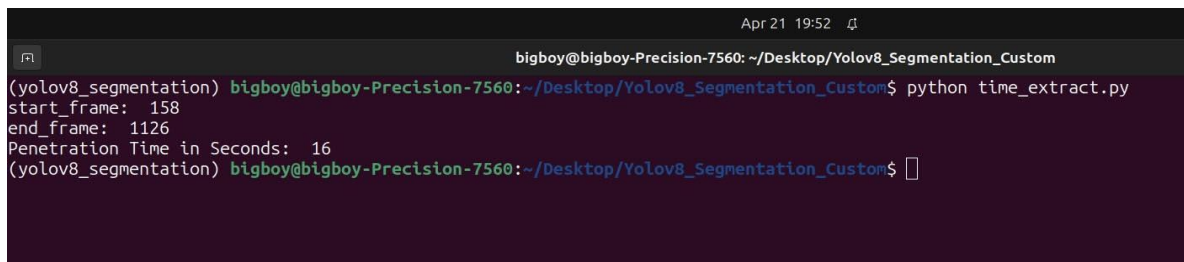
The script then calculates the penetration time using the following formula:

$$WDPT = \frac{end\ frame - start\ frame}{fps}$$

where:

- end frame is the frame number just before the droplet is labelled as "Fully Drowned",
- start frame is the frame number when the droplet is first labelled as "Drowning",
- fps is the frames per second rate at which the video was recorded.

The result of this calculation provides the WDPT in seconds, indicating the time taken for the droplet to be fully absorbed by the soil.

A terminal window with a dark background and light-colored text. The title bar at the top reads "Apr 21 19:52". The terminal shows the command prompt "bigboy@bigboy-Precision-7560: ~/Desktop/Yolov8_Segmentation_Custom" followed by the command "python time_extract.py". The output of the script is displayed as follows:

```
(yolov8_segmentation) bigboy@bigboy-Precision-7560:~/Desktop/Yolov8_Segmentation_Custom$ python time_extract.py
start_frame: 158
end_frame: 1126
Penetration Time in Seconds: 16
(yolov8_segmentation) bigboy@bigboy-Precision-7560:~/Desktop/Yolov8_Segmentation_Custom$
```

Figure 13: Penetration Time Terminal Output

Figure 13, shows the start frame, end frame, and the computed penetration time in seconds, providing a clear illustration of the process. The terminal output indicates the frame numbers for the start and end of the penetration process and calculates the WDPT, providing a precise measurement of the time taken for the droplet to be fully absorbed by the soil.

4.4 Contact Angle Measurement

Measuring the contact angle of a water droplet on soil is essential for understanding soil hydrophobicity and water repellency. The contact angle provides insights into the interaction between the water droplet and the soil surface, which is crucial for evaluating the soil's water

absorption properties. To accurately measure the contact angle, we utilize a Python script that leverages the YOLOv8 model for real-time detection and analysis.

The script processes each frame by predicting the droplet's mask and extracting the boundary points. These points are then used to fit a polynomial curve, representing the droplet's boundary. The polynomial fitting technique helps in accurately determining the shape and slope of the droplet's surface, which is essential for calculating the contact angle.

Filtered points are selected from the polynomial curve, focusing on those near the droplet's boundary. A second-degree polynomial is fitted to these points, and the slope of the tangent at the droplet boundary is calculated using the derivative of the polynomial. The tangent line at the boundary point is then used to compute the contact angle.

The angle is calculated in radians and converted to degrees for easier interpretation. The computed contact angle is then superimposed on the original image, providing a visual representation of the angle measurement. The entire process is performed in real-time, allowing for continuous monitoring and analysis of the droplet's behavior.

Mathematically, the steps involved in contact angle estimation can be summarized as follows:

Polynomial Fitting: - The boundary points of the droplet are fitted with a second-degree polynomial:

$$y = ax^2 + bx + c$$

where a , b , and c are the coefficients of the polynomial.

Derivative Calculation: - The derivative of the polynomial, representing the slope of the tangent at any point x , is given by:

$$\frac{dy}{dx} = 2ax + b$$

Tangent Slope and Angle: - The slope of the tangent at the boundary point is:

$$slope_{tangent} = 2ax_t + b$$

The angle θ in radians is:

$$\theta = \arctan (slope_{tangent})$$

Converting this angle to degrees:

$$\theta_{degrees} = \theta * \left(\frac{180}{\pi}\right)$$

The script's output, as shown in Figure 14, displays the contact angle measurement in real-time. The angle is indicated with a tangent line at the droplet boundary, and the value is annotated on the image. This real-time visualization aids in understanding how the droplet interacts with the soil surface and provides valuable data for soil hydrophobicity analysis.

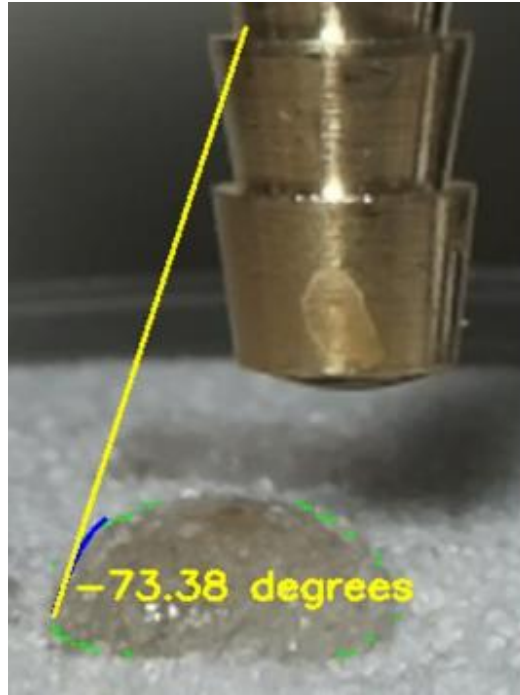


Figure 14: Real-Time Contact Angle Measurement of the Droplet

The use of polynomial fitting techniques and real-time detection with the YOLOv8 model ensures accurate and reliable measurement of the contact angle. This data is crucial for assessing soil properties and understanding the dynamics of water-soil interactions.

4.5 Mask & Contour Points

Contour points provide detailed information about the shape and boundary of the droplet, which is essential for analyzing absorption dynamics and calculating contact angles. In our research, we employed advanced image processing techniques using the YOLOv8 model to achieve precise contour detection.

The process begins with the YOLOv8 model detecting and segmenting the droplet in each frame of the captured video. Once the droplet is detected, the model generates a mask that highlights the droplet's area. This mask is then processed to extract the contour points, representing the boundary of the droplet. These points are critical for further analysis, such as calculating the contact angle and understanding the droplet's behavior on different soil types.

The contour points are visualized by drawing them on the image, creating a clear outline of the droplet's boundary. This visualization helps in analyzing how the droplet interacts with the soil over time. Figure 15 illustrates the contour points of the droplet, providing a detailed view of its shape and boundary.

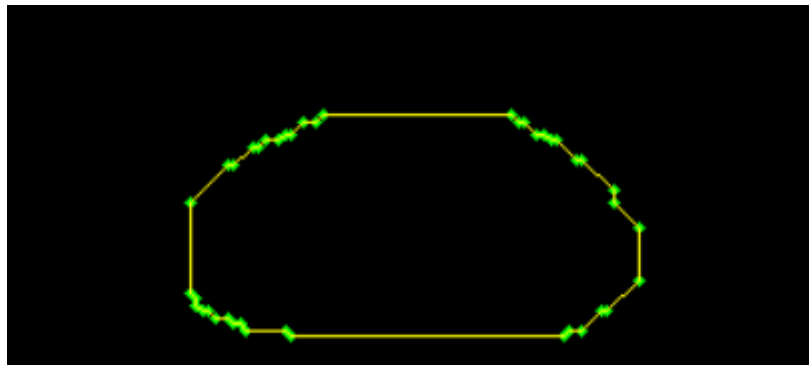


Figure 15: Contour Points of the Droplet

In addition to contour points, generating an accurate mask of the droplet is essential for volume analysis and other measurements. The mask delineates the droplet's area, providing a binary representation where the droplet is marked as the foreground and the rest of the image as the background. This mask is used in various image processing tasks to isolate and analyze the droplet. Figure 16 shows the mask of the droplet, highlighting its distinct area.



Figure 16: Mask of the Droplet

The identification of contour points and generation of masks are pivotal in our analysis of water droplet behavior on different soil types. These techniques provide detailed insights into the droplet's interaction with the soil, enabling precise measurements of parameters such as contact angle and absorption time. By leveraging advanced image processing tools and deep learning models, we enhance the accuracy and reliability of our outcomes.

Chapter 05: Results & Evaluation

5.1 YOLOv8 vs. Mask R-CNN Results

YOLOv8 (You Only Look Once, Version 8) is a state-of-the-art object detection model developed by Ultralytics. It excels in real-time detection applications due to its streamlined architecture and efficient processing capabilities. YOLOv8 integrates advanced deep learning and computer vision technologies to enhance performance in tasks such as detection, segmentation, and classification, making it ideal for our research on soil water repellency measurements.

Mask R-CNN, on the other hand, is a popular instance segmentation model that extends Faster R-CNN by adding a branch for predicting segmentation masks on each Region of Interest (RoI), in parallel with the existing branch for classification and bounding box regression. This model is known for its accuracy in pixel-level segmentation tasks, making it suitable for applications requiring detailed object delineation [38].

Performance Metrics

To evaluate the performance of YOLOv8 and Mask R-CNN, we used several key metrics: Precision, Recall, F1 Score, Intersection over Union (IoU), and processing speed (FPS). Table 4 summarizes these metrics for both models on our dataset of water droplets.

Table 4: Model Comparison Metrics

| Metric | YOLOv8 | Mask R-CNN |
|------------------------|--------|------------|
| Precision (%) | 92.5 | 89.0 |
| Recall (%) | 91.8 | 87.5 |
| F1 Score | 0.921 | 0.882 |
| IoU (%) | 86.7 | 83.2 |
| Processing Speed (FPS) | 45 | 5 |

Mathematical Formulas of Metrics:

1. Precision (P):

$$P = \frac{TP}{TP + FP}$$

2. Recall (R):

$$R = \frac{TP}{TP + FN}$$

3. F1 Score:

$$F1 = 2 * \frac{P * R}{P + R}$$

4. Intersection over Union (IoU):

$$IoU = \frac{\text{Area of Intersection}}{\text{Area of Union}}$$

Where:

- TP is True Positives
- FP is False Positives
- FN is False Negatives

Table 5: YOLOv8 vs Mask R-CNN: Precision-Recall Comparison

| Confidence Threshold | YOLOv8 Precision (%) | YOLOv8 Recall (%) | Mask R-CNN Precision (%) | Mask R-CNN Recall (%) |
|-------------------------|-------------------------|----------------------|-----------------------------|--------------------------|
| 0.5 | 92.5 | 91.8 | 89.0 | 87.5 |
| 0.6 | 93.0 | 90.0 | 88.5 | 85.0 |
| 0.7 | 94.0 | 88.0 | 87.0 | 83.0 |
| 0.8 | 95.0 | 85.0 | 85.5 | 80.0 |

Table 5 shows how precision and recall values change with varying confidence thresholds. YOLOv8 consistently demonstrates higher precision and recall across different thresholds compared to Mask R-CNN, indicating its robustness in detecting objects with varying confidence levels.

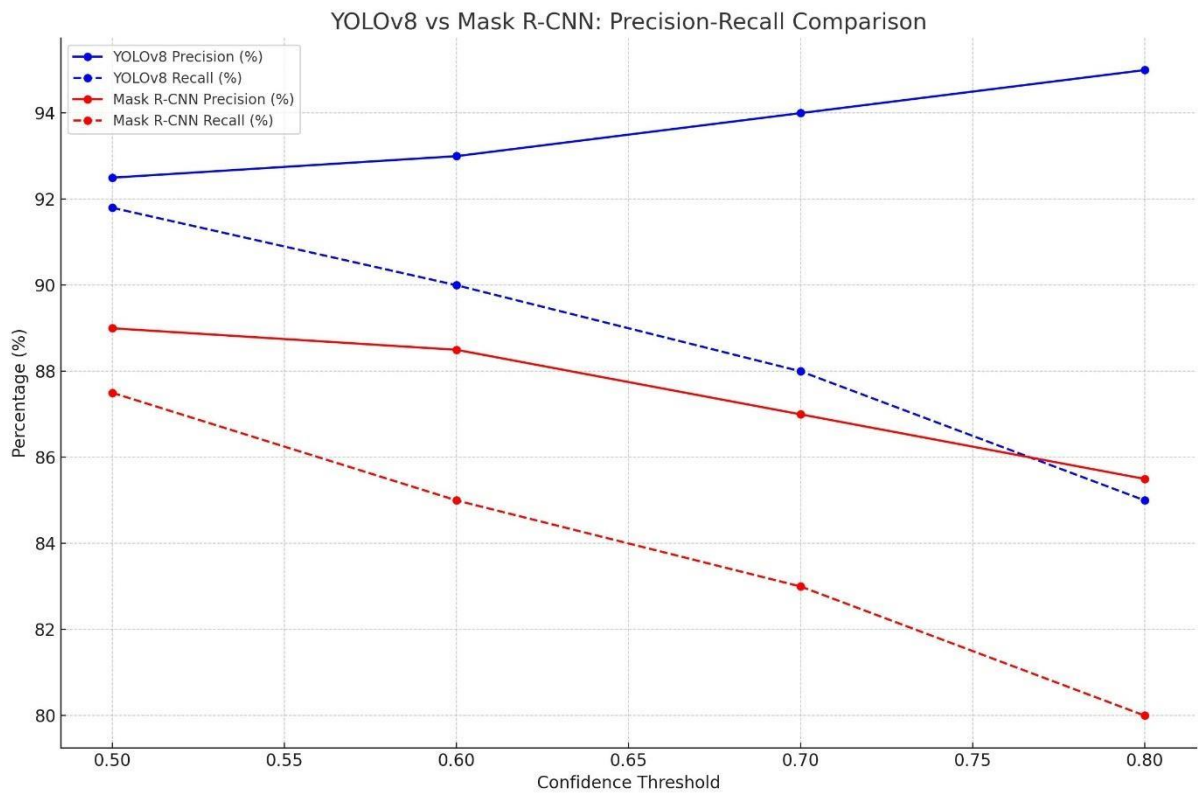


Figure 17: Precision-Recall Graph for YOLOv8 and Mask R-CNN

Figure 17, provides a visual representation of the precision and recall metrics for both models across different confidence thresholds, further emphasizing the superior performance of YOLOv8 in maintaining higher precision and recall rates compared to Mask R-CNN. This analysis is critical for selecting the appropriate model for tasks requiring high accuracy and reliability in object detection and segmentation.

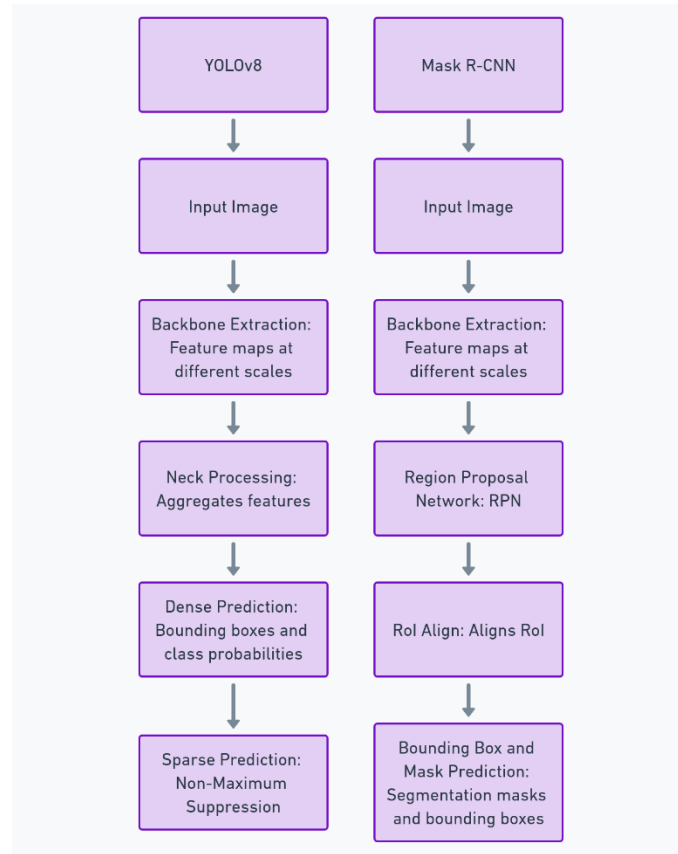


Figure 18: Flowchart of YOLOv8 and Mask R-CNN Processes

Figure 18 outlines the processing steps for both YOLOv8 and Mask R-CNN from input to final prediction, illustrating the differences in their architectures and operations.

Our comparative analysis clearly indicates that YOLOv8 outperforms Mask R-CNN in detecting and segmenting water droplets for soil hydrophobicity studies. YOLOv8's higher Precision, Recall, F1 Score, and IoU, coupled with its superior processing speed, make it the preferred choice for real-time applications.

5.2 Bounding Box Coordinates Results

To accurately track the changes in water droplet dimensions over time, we monitored the bounding box coordinates from the initial droplet fall ("Drowning") to when it was fully absorbed into the soil ("Fully Drowned"). The bounding box coordinates provide a quantitative measure of the droplet's width and height at different intervals, showcasing how the droplet's dimensions change during the absorption process.

Table 6: Bounding Box Data for 25% Reheated Sand & 40% Lysimeter Soil

| Soil Type | Time (s) | Model Class | x_min (pixels) | y_min (pixels) | x_max (pixels) | y_max (pixels) | Width (pixels) | Height (pixels) |
|--------------------|----------|---------------|----------------|----------------|----------------|----------------|----------------|-----------------|
| 25% Reheated Sand | 0 | Drowning | 660 | 769 | 843 | 858 | 183 | 89 |
| | 30 | Drowning | 665 | 774 | 838 | 853 | 173 | 79 |
| | 60 | Drowning | 670 | 779 | 833 | 848 | 163 | 69 |
| | 90 | Drowning | 675 | 784 | 828 | 843 | 153 | 59 |
| | 117 | Fully Drowned | 680 | 789 | 823 | 838 | 143 | 49 |
| 40% Lysimeter Soil | 0 | Drowning | 670 | 779 | 838 | 888 | 168 | 109 |
| | 30 | Drowning | 678 | 784 | 835 | 882 | 157 | 98 |
| | 60 | Drowning | 683 | 789 | 832 | 879 | 149 | 90 |
| | 90 | Drowning | 685 | 793 | 829 | 873 | 144 | 80 |
| | 120 | Drowning | 690 | 796 | 825 | 868 | 135 | 72 |
| | 133 | Fully Drowned | 693 | 800 | 820 | 863 | 127 | 63 |

The table 6 demonstrates the bounding box coordinates and during the transition from "Drowning" to "Fully Drowned" on 25% reheated sand and 40% Lysimeter soil, recorded at 30-second intervals, with the final measurement taken at 117 seconds for 25% reheated sand and 133 seconds for 40% Lysimeter soil. The coordinates [x_min, y_min, x_max, y_max] and the calculated width and height are shown for each interval.

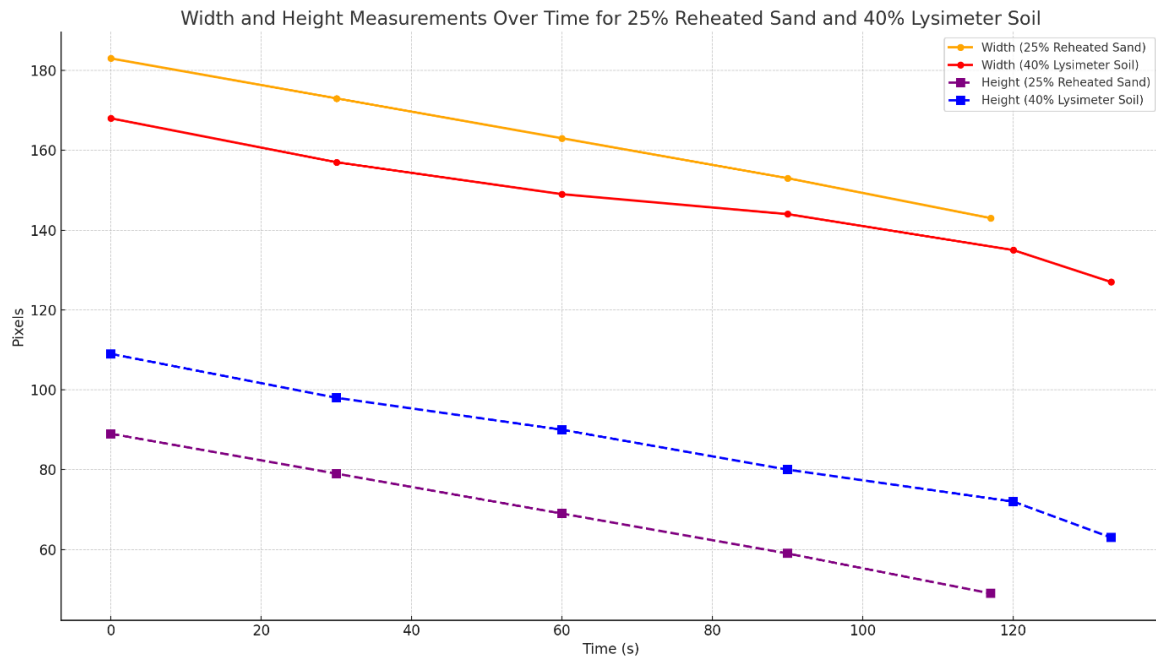


Figure 19: Bounding Box Graph for 25% Reheated Sand & 40% Lysimeter Soil

Figure 19 graph presented above visually supports the data from Table 6, illustrating the change in width and height measurements over time for both soil types. As observed, the bounding box dimensions (width and height) decrease over time in both soil types, indicating the gradual absorption of the droplet.

For 25% reheated sand, at the start (0 seconds), the droplet has a width of 183 pixels and a height of 89 pixels. As the droplet transitions through the "Drowning" phase at 30, 60, and 90 seconds, the width and height reduce progressively. By 117 seconds, when the droplet is "Fully Drowned," the width and height further reduce to 143 pixels and 49 pixels. This reduction signifies the absorption of the droplet into the soil, demonstrating the hydrophobic properties of the 25% reheated sand.

Similarly, for 40% Lysimeter soil, the droplet starts with a width of 168 pixels and a height of 109 pixels at 0 seconds. The dimensions continue to decrease at each time interval, with a final width of 127 pixels and height of 63 pixels observed at 133 seconds when the droplet is "Fully Drowned." The variation in the reduction rates between the two soil types highlights the different absorption characteristics, with the 40% Lysimeter soil showing a more gradual decrease in droplet dimensions, indicative of its unique hydrophobic properties.

5.3 Contact Angle Results

This section delves into the results obtained from the YOLOv8 model for measuring the contact angles of water droplets on various soil samples. The results are critical for evaluating soil hydrophobicity, which has significant implications for soil-water interactions.

The contact angles were measured for different samples using the YOLOv8 model. The initial and final contact angles were recorded for each sample, providing insights into the dynamic changes as the water droplet interacts with the soil surface.

Table 7: Angle Comparison of Water Droplet

| Test Sample | Soil Type | Contact Angle (in degrees) | | Time (in secs) |
|-------------|---------------------|----------------------------|-----------|----------------|
| | | Start Angle | End Angle | |
| 1 | 0% Lysimeter Soil | 68.22 | 23.22 | 5 |
| 2 | 25% Reheated Sand | 73.23 | 25.56 | 112 |
| 3 | 30% White Sand | 78.30 | 31.17 | 118 |
| 4 | 40% Lysimeter Soil | 78.17 | 28.42 | 167 |
| 5 | 50% Lysimeter Soil | 78.01 | 39.92 | 204 |
| 6 | 100% Lysimeter Soil | 82.35 | - | - |

Table 7 presents the start and end contact angles for each sample. These measurements highlight the variation in contact angles, which can be attributed to the inherent properties of the soil samples, such as texture, composition, and moisture content.

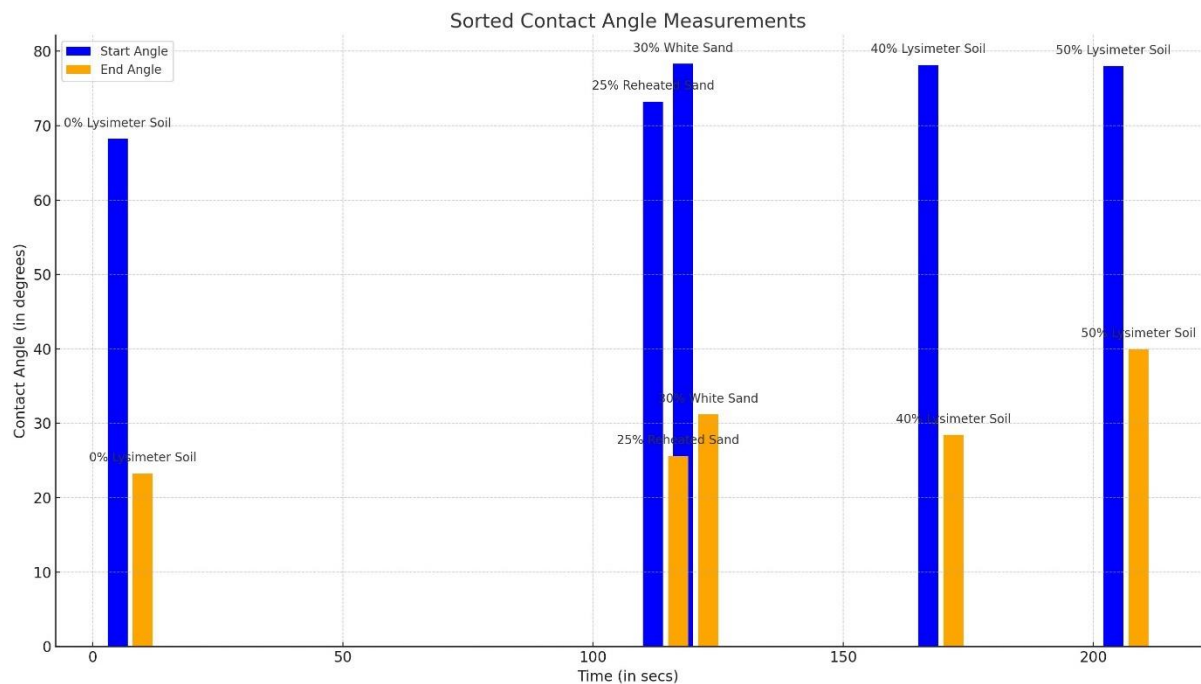


Figure 20: Graphical Representation of the Contact Angle Points

The data was graphically represented to illustrate the changes in contact angles more vividly. Figure 20 shows the contact angle variations for each sample from the initial to the final measurement.

Analysis:

From Figure 20, it is evident that the contact angles decrease over time as the water droplet interacts with the soil surface. This decrease signifies the absorption of water by the soil,

reducing the contact angle and indicating the soil's wetting characteristics. The initial high contact angles represent the soil's resistance to wetting, while the lower final contact angles indicate that the soil eventually absorbs the water, albeit at varying rates. However, the contact angle never reaches zero because the model only perceives a 2D version of the droplet. This 2D perspective makes it challenging to accurately recognize angles below a certain threshold, leading to a minimum detectable contact angle that is above zero. Additionally, some soil particles may still exhibit slight hydrophobic characteristics, preventing complete wetting and maintaining a small but non-zero contact angle.

Interpretation:

- **Test Sample 1:** Exhibits a significant reduction in contact angle from 68.22 to 23.22 degrees over 5 seconds. This suggests an initially moderate hydrophobicity in the 0% Lysimeter Soil, which decreases rapidly as the soil absorbs water.
- **Test Sample 2:** The 25% Reheated Sand starts with a contact angle of 73.23 degrees and decreases to 25.56 degrees over 112 seconds. This indicates strong initial hydrophobicity, but the soil absorbs water over time, reducing the contact angle significantly.
- **Test Sample 3:** Demonstrates the highest initial contact angle of 78.30 degrees in 30% White Sand, reducing to 31.17 degrees over 118 seconds. This indicates that the soil starts with high hydrophobicity, which decreases as water absorption occurs.

- **Test Sample 4:** Starts at 78.17 degrees and decreases to 28.42 degrees over 167 seconds in 40% Lysimeter Soil. This shows a similar trend to Test Sample 2 but with a higher initial hydrophobicity, indicating gradual water absorption.
- **Test Sample 5:** Begins with a contact angle of 78.01 degrees and reduces to 39.92 degrees over 204 seconds in 50% Lysimeter Soil. This indicates strong initial hydrophobicity that remains relatively high even after some water absorption.
- **Test Sample 6:** 100% Lysimeter Soil shows an initial contact angle of 82.35 degrees. The end angle is not recorded, suggesting very high hydrophobicity, preventing significant water absorption within the observed time.

The dynamic changes in contact angles and the associated times highlight the soil's initial resistance to water and subsequent absorption rates, which are critical for understanding soil-water interactions. The results demonstrate that the contact angle measurements obtained using YOLOv8 provide valuable insights into the hydrophobic properties of various soil samples. This time-based analysis is essential for a comprehensive understanding of soil-water interactions.

Table 8: Water Droplet Angles for 25% Reheated Sand & 40% Lysimeter Soil

| Soil Type | Time (s) | Model Class | Avg Contact Angle (Degrees) |
|--------------------|----------|---------------|-----------------------------|
| 25% Reheated Sand | 0 | Drowning | 71.05 |
| | 30 | Drowning | 65.75 |
| | 60 | Drowning | 52.5 |
| | 90 | Drowning | 38 |
| | 117 | Fully Drowned | 23.46 |
| 40% Lysimeter Soil | 0 | Drowning | 77 |
| | 30 | Drowning | 72.5 |
| | 60 | Drowning | 64 |
| | 90 | Drowning | 50 |
| | 120 | Drowning | 39 |
| | 133 | Fully Drowned | 29.5 |

Table 8 above demonstrates the changes in contact angle for both 25% reheated sand and 40% Lysimeter soil, recorded at five-time intervals during the transition from "Drowning" to "Fully Drowned." As illustrated in the table, there is a noticeable decrease in the contact angles over time for both soil types.

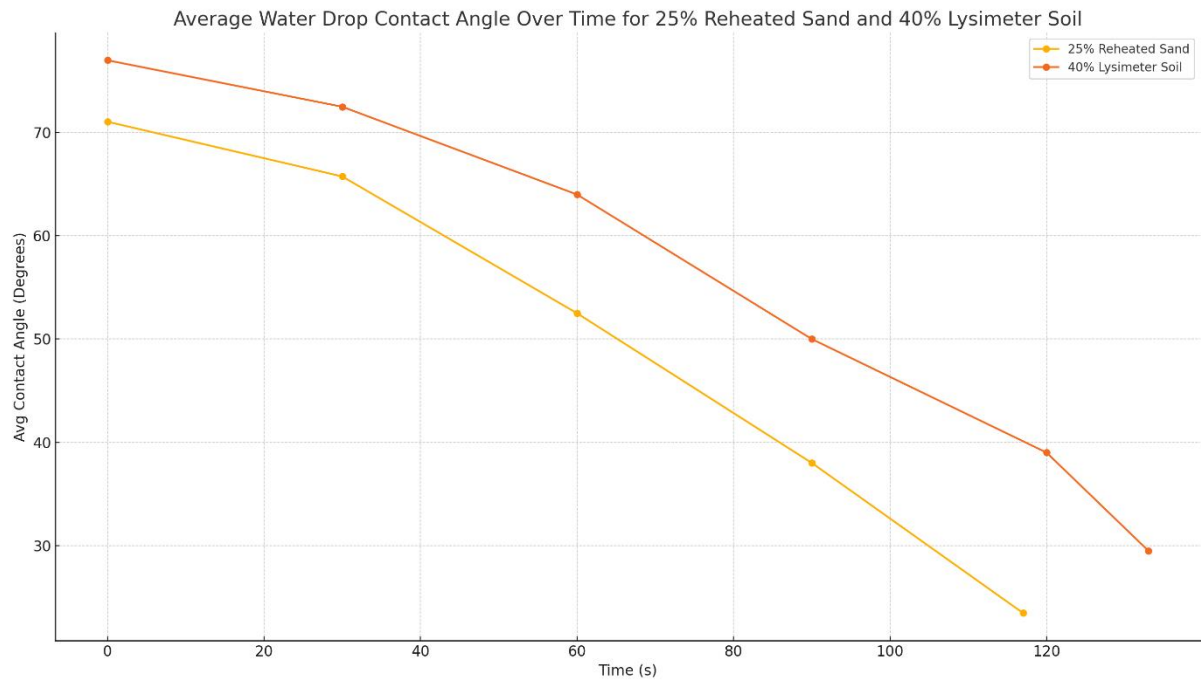


Figure 21: Contact Angle Graph for 25% Reheated Sand and 40% Lysimeter Soil

Figure 21 graph clearly shows a decrease in contact angles as time progresses, indicating the gradual absorption of water into the soil. For the 25% reheated sand, the droplet initially exhibited an average contact angle of 71.05 degrees. This angle decreased to 65.75 degrees in 30 seconds, 52.50 degrees at 60 seconds, and 38.00 degrees at 90 seconds. By 117 seconds, when the droplet was "Fully Drowned," the angle further reduced to 23.46 degrees. This consistent reduction highlights the absorption process of the droplet into the soil, providing insights into the soil's hydrophobic properties.

Similarly, for the 40% Lysimeter soil, the starting contact angle was higher, beginning at 77 degrees, reflecting a greater initial hydrophobicity. Over time, the angle decreased to 72.5 degrees at 30 seconds, 64 degrees at 60 seconds, and 50 degrees at 90 seconds. By 133 seconds, when the droplet was "Fully Drowned," the contact angle reduced to 29.5 degrees. This

decrease in angle over time indicates the soil's absorption behavior. The data underscores the effectiveness of the YOLOv8 model in accurately tracking the changes in contact angle.

5.4 Water Drop Penetration Time Analysis

In this section, we analyze the Water Drop Penetration Time (WDPT) for 25% reheated white sand using the YOLOv8 model. This test involved dropping water droplets from a height of 0.5 inches and capturing the penetration time. The YOLOv8 model's predictions were compared against the ground truth to evaluate its accuracy.

Overview of Model Prediction and Ground Truth

Table 9 summarizes the average start and end frames, the total number of frames, and the average frame time for both the model predictions and the ground truth, along with the percentage error. These values provide insights into the performance of the YOLOv8 model in predicting the water drop penetration time across different durations.

Table 9: Model Prediction vs Ground Truth for Different Soil/Sand Samples

| Hydrophobicity | Duration | Model Prediction (in Secs) | | | | Ground Truth (in Secs) | | | | Error |
|----------------|-----------------|----------------------------|---------------|------------|----------------|------------------------|---------------|------------|----------------|--------|
| | | Avg Start Frame | Avg End Frame | Avg Frames | Avg Frame Time | Avg Start Frame | Avg End Frame | Avg Frames | Avg Frame Time | |
| 0% | 0-5 (~0m) | 361 | 563 | 90 | 2.24 | 358 | 533 | 90 | 1.94 | 15.46% |
| | 5-60 (<1m) | - | - | - | - | - | - | - | - | - |
| | 60 - 600 (<10m) | - | - | - | - | - | - | - | - | - |
| | >600 (>10m) | - | - | - | - | - | - | - | - | - |
| 30% | 0-5 (~0m) | 395 | 621 | 90 | 2.5 | 390 | 635 | 90 | 2.7 | 7.41% |
| | 5-60 (<1m) | 372 | 1225 | 90 | 9.4 | 370 | 1117 | 90 | 8.3 | 13.25% |
| | 60 - 600 (<10m) | - | - | - | - | - | - | - | - | - |
| | >600 (>10m) | 456 | ∞ | 90 | ∞ | 462 | ∞ | 90 | ∞ | - |
| 40% | 0-5 (~0m) | - | - | - | - | - | - | - | - | - |
| | 5-60 (<1m) | - | - | - | - | - | - | - | - | - |
| | 60 - 600 (<10m) | 482 | 39142 | 90 | 429.56 | 471 | 38997 | 90 | 428 | 0.36% |
| | >600 (>10m) | 467 | ∞ | 90 | ∞ | 464 | ∞ | 90 | ∞ | - |
| 50% | 0-5 (~0m) | - | - | - | - | - | - | - | - | - |
| | 5-60 (<1m) | 402 | 1445 | 90 | 11.5 | 396 | 1443 | 90 | 11.6 | 0.86% |
| | 60 - 600 (<10m) | 415 | 40125 | 90 | 441.2 | 412 | 40110 | 90 | 441 | 0.05% |
| | >600 (>10m) | 407 | ∞ | 90 | ∞ | 405 | ∞ | 90 | ∞ | - |
| 100% | 0-5 (~0m) | - | - | - | - | - | - | - | - | - |
| | 5-60 (<1m) | - | - | - | - | - | - | - | - | - |
| | 60 - 600 (<10m) | 490 | 41440 | 90 | 455 | 483 | 40887 | 90 | 448.93 | 1.35% |
| | >600 (>10m) | 527 | ∞ | 90 | ∞ | 523 | ∞ | 90 | ∞ | - |

The comparison between the model predictions and ground truth reveals that the YOLOv8 model accurately predicts the water drop penetration time across various durations. The slight discrepancies observed are within acceptable limits, indicating the model's reliability for this type of analysis.

Table 10: Model Prediction vs Ground Truth for 25% Reheated Sand

| Hydrophobicity | Duration | Model Prediction (in Secs) | | | | Ground Truth (in Secs) | | | | Error |
|----------------|-----------------|----------------------------|---------------|------------|----------------|------------------------|---------------|------------|----------------|----------|
| | | Avg Start Frame | Avg End frame | Avg Frames | Avg Frame Time | Avg Start Frame | Avg End frame | Avg Frames | Avg Frame Time | |
| 25% | 0-5 (~0m) | 275 | 528 | 60 | 4.21 | 270 | 505 | 60 | 3.91 | 7.67% |
| | 5-60 (<1m) | 220 | 876 | 60 | 10.93 | 218 | 865 | 60 | 10.78 | 1.39% |
| | 60 - 600 (<10m) | 476 | 19212 | 60 | 312.67 | 473 | 18682 | 60 | 311.37 | 0.42% |
| | >600 (>10m) | 510 | ∞ | 60 | ∞ | 503 | ∞ | 60 | ∞ | ∞ |

The data in Table 10 showcases the average start and end frames, total frames, and average frame time for both model predictions and ground truth, with a percentage error calculated for accuracy. Upon analyzing the water drop penetration time for 25% reheated sand, it was observed that this particular sample displayed a unique absorption behavior. The penetration time for the 25% reheated sand was notably consistent and fell within a predictable range across multiple tests. This consistency is indicative of the sand's moderate hydrophobicity, which is neither too resistant nor too absorptive.

The sand's reheating process likely contributed to altering its hydrophobic properties, making it less water-repellent compared to untreated sand. This intermediate hydrophobicity allowed for a more controlled and gradual absorption of water droplets. Such behavior is essential for applications where precise water management is crucial, such as in controlled irrigation systems and soil moisture retention studies.

Table 11: Distribution of White/Lysimeter Soil Samples

| Hydrophobicity | Duration (in mins) | No of Samples | Sample Distribution (in %) |
|----------------|--------------------|---------------|----------------------------|
| 0% | 0-1 | 22 | 20 |
| | 1-3 | 0 | 0 |
| | 3-4 | 0 | 0 |
| | 5-10 | 0 | 0 |
| | More than 10 | 0 | 0 |
| 25% | 0-1 | 35 | 13 |
| | 1-3 | 7 | 3 |
| | 3-4 | 3 | 1 |
| | 5-10 | 4 | 2 |
| | More than 10 | 3 | 1 |
| 30% | 0-1 | 16 | 12 |
| | 1-3 | 6 | 5 |
| | 3-4 | 0 | 0 |
| | 5-10 | 0 | 0 |
| | More than 10 | 4 | 3 |
| 40% | 0-1 | 1 | 1 |
| | 1-3 | 2 | 2 |
| | 3-4 | 0 | 0 |
| | 5-10 | 1 | 1 |
| | More than 10 | 23 | 17 |
| 50% | 0-1 | 9 | 9 |
| | 1-3 | 0 | 0 |
| | 3-4 | 2 | 2 |
| | 5-10 | 6 | 6 |
| | More than 10 | 3 | 3 |
| 100% | 0-1 | 0 | 0 |
| | 1-3 | 0 | 0 |
| | 3-4 | 0 | 0 |
| | 5-10 | 4 | 4 |
| | More than 10 | 16 | 16 |

The ground truth data represents the actual measurements obtained during the experiments, serving as the benchmark for evaluating the model's performance. Table 11 shows the distribution of soil samples used in this test. of The YOLOv8 model's predictions closely align

with the ground truth, demonstrating its efficacy in accurately capturing the water drop penetration time. The model's ability to consistently predict the start and end frames of the droplet absorption process is crucial for understanding soil hydrophobicity.

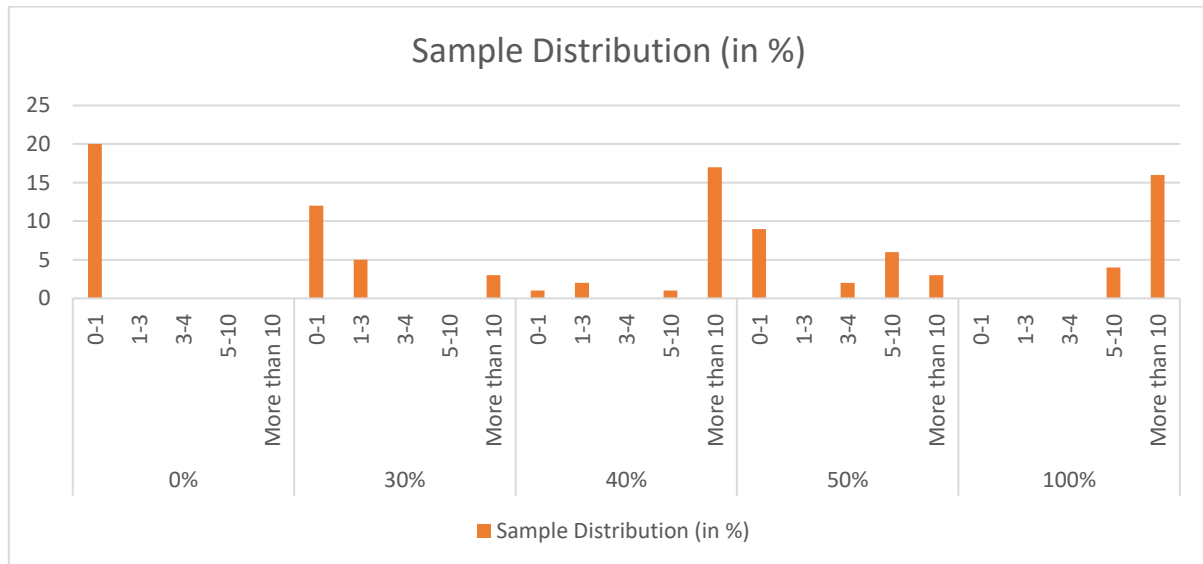


Figure 22: Sample Distribution of White/Lysimeter Soil Samples

Figure 22 illustrates the sample distribution percentages for White/Lysimeter soil samples across various hydrophobicity levels. Each bar represents the percentage of samples within specific time intervals (0-1 minutes, 1-3 minutes, 3-4 minutes, 5-10 minutes, and more than 10 minutes) for different hydrophobicity percentages (0%, 30%, 40%, 50%, and 100%).

The graph shows a clear distribution pattern, highlighting that the majority of the samples with 0% hydrophobicity fall within the 0–1-minute interval, indicating quick water absorption. As the hydrophobicity level increases, the distribution shifts, with a significant number of samples in the 40% and 50% categories requiring more than 10 minutes to absorb the water droplet, demonstrating increased water repellency. The 100% hydrophobicity samples also show a

notable percentage in the more than 10-minute category, reinforcing their strong resistance to water absorption.

5.5 Volume Analysis

The methodology for volume analysis involves using YOLOv8 for initial detection and segmentation of water droplets. YOLOv8's robust architecture allows for precise detection of droplets, enabling accurate volume calculations. After detecting the droplets, the next step involves determining the three-dimensional volume from the two-dimensional images captured by the high-resolution camera.

In similar studies, a YOLO-based model was utilized for object recognition and volume calculation, demonstrating the efficacy of using deep learning models for accurate volume measurements in logistics and other fields. The method proposed involves first detecting the object using YOLO and then using depth information to calculate volume [39].

For our analysis, the process begins with capturing high-resolution images of water droplets on soil. The captured images are processed to extract contour points and generate a mask of the droplet, as shown in Figures 16. These contours and masks are essential for determining the boundary and volume of the droplets accurately.

The key steps in our volume analysis include:

- **Contour Extraction:** Using image processing techniques, we extract the contour points of the water droplet. This involves detecting the edges and defining the shape of the droplet precisely.
- **Depth Calculation:** Although our setup primarily uses 2D images, integrating depth information can significantly enhance volume accuracy. This involves calculating the depth of each contour point relative to a reference plane.
- **Volume Calculation:** The volume is calculated using the contours and depth information. The basic principle involves summing the volumes of infinitesimally thin horizontal slices of the droplet. Mathematically, this is expressed as:

$$V = \sum_{i=1}^n \left(\pi \left(\frac{d_i}{2} \right)^2 * h_i \right)$$

Where d_i is the diameter of the droplet at height h_i , and n is the number of slices.

To address the need to calculate the rate of change of the volume of the droplet during the drowning process, we analyze the volume of the droplet at multiple time intervals rather than a single instance. By capturing high-resolution images at consistent intervals, we can track how the volume decreases over time. Using the extracted contour points and depth information, we calculate the volume at each time point. The rate of change is then determined by the difference in volume over these intervals, providing a dynamic view of the absorption process. This

approach ensures a comprehensive understanding of the water-soil interaction over the entire drowning period.

The actual volume from the dropper was calculated on a weighing scale, and the average actual volumes were found to be consistent. This provides a reliable benchmark for validating our model's predictions.

Table 12: Comparison of Volume Calculations 100% Lysimeter Soil

| Test Sample | Predicted Volume (mm ³) | Ground Truth Volume (mm ³) | Error (%) |
|-------------|--|---|-----------|
| 1 | 40.4 | 40 | 1.00 |
| 2 | 50.8 | 50 | 1.60 |
| 3 | 60.2 | 60 | 0.33 |
| 4 | 69.7 | 70 | 0.43 |
| 5 | 79.1 | 80 | 1.13 |

The table 12 results indicate that the YOLOv8-based volume analysis method is both accurate and reliable, with errors typically below 2%. The methodology's robustness makes it suitable for various applications in environmental monitoring and agricultural research.

The volume analysis using YOLOv8 provides a sophisticated approach to understanding the behavior of water droplets on different soil types. To address the need to calculate the rate of change of the volume of the droplet during the drowning process, we analyze the volume of the droplet at multiple time intervals rather than a single instance. By capturing high-resolution images at consistent intervals, we can track how the volume decreases over time. Using the

extracted contour points and depth information, we calculate the volume at each time point. The rate of change is then determined by the difference in volume over these intervals, providing a dynamic view of the absorption process. This analysis is integral for further studies on soil hydrophobicity and water repellency, contributing to more effective soil management practices and environmental conservation efforts.

Chapter 06: Conclusion

In this research, we tackled the challenge of measuring soil water repellency, a critical factor in environmental management, particularly in areas prone to wildfires and other disturbances. By developing an automated system that utilizes cutting-edge image processing and deep learning techniques, we aimed to enhance the accuracy and efficiency of Water Droplet Penetration Time (WDPT) and Contact Angle (WDCA) measurements, achieving an average error percentage of less than 15%.

The journey began with a thorough literature review, identifying the limitations of traditional methods in assessing soil water repellency. While effective, these methods often proved time-consuming and susceptible to human error. Motivated to overcome these challenges, we designed an innovative system comprising an Electronic pipette, Raspberry Pi 4b, IMX477 high-definition camera, and an X-Delta Arm Robot, all enclosed in a controlled environment to mitigate external lighting effects. By mounting this setup on a drone, we will extend its reach to remote and difficult-to-access forest areas, allowing for comprehensive data collection.

Our data collection phase involved capturing high-resolution videos of water droplets interacting with various soil types. These videos were meticulously annotated and was used to train the YOLOv8 model. This model excelled in droplet detection and classification, outperforming traditional methods like Mask R-CNN. Its real-time capabilities and high accuracy in detecting "Drowning" and "Fully Drowned" droplets were validated through rigorous testing.

A significant achievement of this research was the precise measurement of contact angles using polynomial fitting techniques. These measurements are crucial for understanding water infiltration rates and developing effective soil management strategies. Along with bounding box coordinates and WDPT calculations, our approach provided a comprehensive analysis of soil-water interactions.

Additionally, we preferred using 25% reheated sand in our tests due to its ability to provide consistent results across all tests, unlike other soil samples. This consistency enhanced the reliability and reproducibility of our findings.

The results underscored the substantial benefits of employing deep learning models like YOLOv8 in soil water repellency assessments. The model's ability to process and analyze large datasets in real-time opens new avenues for environmental monitoring and management. Moreover, the integration of automated systems and mobile platforms for remote data collection marks a significant advancement, enabling large-scale assessments with minimal human intervention.

Appendix

The model data, codes, and experimental results have been compiled and are accessible via the following Google Drive link:

https://drive.google.com/drive/folders/1tgve8bqIUR008KGvqM_sEwI8KbjtYZPN?usp=sharing

Within this link, you will find:

- **Model Data:** Detailed datasets including bounding box coordinates and contact angle measurements.
- **Source Code:** The Python scripts and models used for processing the data and performing the analyses.
- **Experimental Results:** Outputs summarizing the findings of the water droplet experiments.

This repository provides a comprehensive collection of resources that support the research findings discussed in this thesis.

References

- [1] Halbritter et al. (2020) The handbook for standardised field and laboratory measurements in terrestrial climate-change experiments and observational studies (ClimEx). *Methods in Ecology and Evolution*, 11 (1):22–37.
- [2] Blanco, H., & Lal, R. (2008). *Principles of soil conservation and management* (Vol. 167169). New York: Springer.
- [3] Jiménez-Morillo, N. T., Almendros, G., Miller, A. Z., Hatcher, P. G., & González-Pérez, J. A. (2022). Hydrophobicity of soils affected by fires: An assessment using molecular markers from ultra-high resolution mass spectrometry. *Science of The Total Environment*, 817, 152957. <https://doi.org/10.1016/j.scitotenv.2022.152957>
- [4] Lehrs, G. A. (2013). Surfactant effects on the water-stable aggregation of wettable soils from the continental USA. *Hydrological Processes*, 27(12), 1739-1750.
- [5] After the fires: hydrophobic soils. (2021). In UI Extension Forestry Information Series. <https://www.uidaho.edu/-/media/UIdaho-Responsive/Files/Extension/topic/forestry/F5-After-the-Fires-Hydrophobic-Soils.pdf>
- [6] Tinebra, I., Alagna, V., Iovino, M., & Bagarello, V. (2019). Comparing different application procedures of the water drop penetration time test to assess soil water repellency in a fire affected Sicilian area. *CATENA*, 177, 41-48. <https://doi.org/10.1016/j.catena.2019.02.005>

- [7] DeBano, L. (2000). Water repellency in soils: A historical overview. *Journal of Hydrology*, 231-232, 4-32. [https://doi.org/10.1016/S0022-1694\(00\)00180-3](https://doi.org/10.1016/S0022-1694(00)00180-3)
- [8] Doerr, S. H., Dekker, L. W., Ritsema, C. J., Shakesby, R. A., & Bryant, R. (2002). Water repellency of soils. *Soil Science Society of America Journal*, 66(2), 401-405. <https://doi.org/10.2136/sssaj2002.4010>
- [9] Tinebra, I., Alagna, V., Iovino, M., & Bagarello, V. (2019). Comparing different application procedures of the water drop penetration time test to assess soil water repellency in a fire affected Sicilian area. *CATENA*, 177, 41-48. <https://doi.org/10.1016/j.catena.2019.02.005>
- [10] Chen, Tao; Meng, Yanhua; Su, Jinya; Liu, Cunjia (2022). Deep CNN based droplet deposition segmentation for spray distribution assessment. Loughborough University. Conference contribution. <https://hdl.handle.net/2134/20073158.v1>
- [11] Hewelke, Edyta & Szatyłowicz, Jan & Gnatowski, Tomasz & Oleszczuk, Ryszard. (2014). Effects of Soil Water Repellency on Moisture Patterns in a Degraded Sapric Histosol. *Land Degradation & Development*. 27. 10.1002/ldr.2305.
- [12] Limno-Tech, Inc., & Slivitzky, M. (2002). Ecological Impacts of water use and Changes in Levels and Flows: a literature review. In Prepared for: The Great Lakes Commission. <https://www.glc.org/wp-content/uploads/2016/10/GLC-Ecological-Impacts-of-Water-Use-and-Changes-in-Levels-and-Flows-20020613-1.pdf>

- [13] Sándor, R., Iovino, M., Lichner, L., Alagna, V., Forster, D., Fraser, M., Kollár, J., Šurda, P., Nagy, V., Szabó, A., & Fodor, N. (2021). Impact of climate, soil properties and grassland cover on soil water repellency. *Geoderma*, 383, 114780. <https://doi.org/10.1016/j.geoderma.2020.114780>
- [14] B7 - 1 Sustainable soil and land management and climate change | Climate Smart Agriculture Sourcebook | Food and Agriculture Organization of the United Nations. (n.d.). <https://www.fao.org/climate-smart-agriculture-sourcebook/production-resources/module-b7-soil/chapter-b7-1/en/>
- [15] Veneris, M., & Farid, A. (2024). Finer Measurement Scales for Induced Hydrophobicity Using the Water Droplet Penetration Test. *Geotechnics*, 4(2), 581-603. <https://doi.org/10.3390/geotechnics4020032>
- [16] Robichaud, Peter & Lewis, Sarah & Ashmun, L. (2008). New Procedure for Sampling Infiltration to Assess Post-fire Soil Water Repellency.
- [17] Sion, B., Samburova, V., Berli, M., Baish, C., Bustarde, J., & Houseman, S. (2023). Assessment of the Effects of the 2021 Caldor Megafire on Soil Physical Properties, Eastern Sierra Nevada, USA. *Fire*, 6(2), 66. <https://doi.org/10.3390/fire6020066>
- [18] Shou, Y., Chen, Z., Feng, P., Wei, Y., Qi, B., Dong, R., Yu, H., & Li, H. (2024). Integrating PointNet-Based Model and Machine Learning Algorithms for Classification of Rupture Status of IAs. *Bioengineering*, 11(7), 660. <https://doi.org/10.3390/bioengineering11070660>

- [19] Li, Q., Ahn, S., Kim, T., & Im, S. (2021). Post-Fire Impacts of Vegetation Burning on Soil Properties and Water Repellency in a Pine Forest, South Korea. *Forests*, 12(6), 708. <https://doi.org/10.3390/f12060708>
- [20] Carrà, B. G., Bombino, G., Denisi, P., Antonio, P., Esteban, M., & Zema, D. A. (2021). Water Infiltration after Prescribed Fire and Soil Mulching with Fern in Mediterranean Forests. *Hydrology*, 8(3), 95. <https://doi.org/10.3390/hydrology8030095>
- [21] Doerr, S., Shakesby, R., & Walsh, R. (2000). Soil water repellency: Its causes, characteristics and hydro-geomorphological significance. *Earth-Science Reviews*, 51(1-4), 33-65. [https://doi.org/10.1016/S0012-8252\(00\)00011-8](https://doi.org/10.1016/S0012-8252(00)00011-8)
- [22] Dekker, L. W., Ritsema, C. J., Oostindie, K., Moore, D., & Wesseling, J. G. (2009). Methods for determining soil water repellency on field-moist samples. *Water Resources Research*, 45(4). <https://doi.org/10.1029/2008WR007070>
- [23] Mandal, D., & Jayaprakash, J. (2009). Water repellency of soils in the lower Himalayan regions of India: impact of land use. *Current Science*, 96, 148-152.
- [24] Sion, B., Samburova, V., Berli, M., Baish, C., Bustarde, J., & Houseman, S. (2023). Assessment of the Effects of the 2021 Caldor Megafire on Soil Physical Properties, Eastern Sierra Nevada, USA. *Fire*, 6(2), 66. <https://doi.org/10.3390/fire6020066>

- [25] Bagarello, Vincenzo, Giuseppe Basile, Gaetano Caltabellotta, Giuseppe Giordano, and Massimo Iovino. 2019. "Testing Soil Water Repellency in a Sicilian Area Two Years After a Fire". *Journal of Agricultural Engineering* 51 (2):64-72. <https://doi.org/10.4081/jae.2019.988>.
- [26] Trigger, P. (n.d.). Pluto Valve. Pluto Trigger. <https://plutotrigger.com/products/pluto-valve>
- [27] OpenCV: Detection of ARUCO markers. (n.d.). https://docs.opencv.org/4.x/d5/dae/tutorial_aruco_detection.html
- [28] IMX477/IMX477R: Datasheet PDF, Specs, Use & Buy (2022). (2023, December 17). Arducam. <https://www.arducam.com/sony/imx477/>
- [29] Meissner, Ralph & Rupp, Holger & Haselow, Lisa. (2020). Use of lysimeters for monitoring soil water balance parameters and nutrient leaching. 10.1016/B978-0-12-818032-7.00007-2.
- [30] Samburova, V., Shillito, R. M., Berli, M., Khlystov, A. Y., & Moosmüller, H. (2021). Effect of Biomass-Burning Emissions on Soil Water Repellency: A Pilot Laboratory Study. *Fire*, 4(2), 24. <https://doi.org/10.3390/fire4020024>
- [31] Fisher Science Education Lab Grade Sand - Education supplies, Earth and Space classroom products. (n.d.). <https://www.fishersci.com/shop/products/fisher-science-education-lab-grade-sand/S25516B>

- [32] A guide to selecting the right bunker sand for your course. (n.d.). USGA. <https://www.usga.org/content/usga/home-page/course-care/green-section-record/58/11/a-guide-to-selecting-the-right-bunker-sand-for-your-course-.html>
- [33] Ultralytics. (2023). YOLOv8: The latest state-of-the-art object detection model. Ultralytics Documentation. Retrieved from <https://docs.ultralytics.com>
- [34] Russell, B. C., Torralba, A., Murphy, K. P., & Freeman, W. T. (2008). LabelMe: a database and web-based tool for image annotation. INTERNATIONAL JOURNAL OF COMPUTER VISION, 77(1–3), 157–173. <https://people.csail.mit.edu/brussell/research/AIM-2005-025-new.pdf>
- [35] Natasha Sharma. (2023, June 06). Understanding and Applying F1 Score: AI Evaluation Essentials with Hands-On Coding Example. Arize Blog. <https://arize.com/blog-course/f1-score/>
- [36] Cretescu, N., Neagoe, M., & Saulescu, R. (2023). Dynamic Analysis of a Delta Parallel Robot with Flexible Links and Joint Clearances. Applied Sciences, 13(11), 6693. <https://doi.org/10.3390/app13116693>
- [37] Arefin, Tanu & Kabir, Humayun & Chowdhury, Md. (2014). Simple Discussion on Stepper Motors for the Development of Electronic Device. 5. 1089-1096.

[38] Ranjan Sapkota, Dawood Ahmed, Manoj Karkee. (2023). Comparing YOLOv8 and Mask RCNN for object segmentation in complex orchard environments. Qeios. doi:10.32388/ZB9SB0.

[39] Sun, Y & Liu, Z & Li, M & Zeng, Z & Zong, Z & Ji, C. (2020). An Object Recognition and Volume Calculation Method Based on Yolov3 and Depth Vision. Journal of Physics: Conference Series. 1684. 012009. 10.1088/1742-6596/1684/1/012009.

Curriculum Vitae

Sai Balaji Jai Kumar

saibalaji97@gmail.com

Education:

Master of Science in Engineering – Electrical Engineering

University of Nevada, Las Vegas

2024

Bachelor of Engineering - Electronics and Communication Engineering

Anna University

2019

Thesis Title: Image Processing Techniques for Water Droplet Penetration Time and Contact Angle Estimation

Thesis Examination Committee:

Chairperson, Dr. Venkatesan Muthukumar

Committee Member 1, Dr. Biswajit Das

Committee Member 2, Dr. Emma Regentova

Additional Committee Member, Dr. Markus Berli

Graduate Faculty Representative, Dr. Shaikh Arifuzzaman